Advances in Applied Energy 10 (2023) 100134

Contents lists available at ScienceDirect

Advances in Applied Energy

journal homepage: www.elsevier.com/locate/adapen

# Implications of a Paris-proof scenario for future supply of weather-dependent variable renewable energy in Europe

Jing Hu[a,*], Vinzenz Koning[a,b], Thomas Bosshard[c], Robert Harmsen[a], Wina Crijns-Graus[a], Ernst Worrell[a], Machteld van den Broek[d]

[a] Copernicus Institute of Sustainable Development, Utrecht University, Heidelberglaan 2, 3584 CS Utrecht, The Netherlands
[b] Centre for Complex Systems Studies, Utrecht University, Minnaertgebouw, Leuvenlaan 4, 3584 CE Utrecht, , The Netherlands
[c] Swedish Meteorological and Hydrological Institute, Folkborgsvägen, 601 76 Norrköping, Sweden
[d] Faculty of Science and Engineering, University of Groningen, Nijenborgh 9, 9747 AG Groningen, The Netherlands

ARTICLE INFO

*Keywords:*
Energy
Renewable energy
Climate change
Paris Agreement
Wind
Solar
Energy droughts
Dunkelflaute
Wind-solar complementarity
Cross-border
Energy system
Climate impact
Capacity factor
VRE
Energy conversion
Copula
Tail dependence
Futute climate
Europe
Spectral analysis
Power system

ABSTRACT

To meet the European Union's 2050 climate neutrality target, future electricity generation is expected to largely rely on variable renewable energy (VRE). VRE supply, being dependant on weather, is susceptible to changing climate conditions. Based on spatiotemporally explicit climate data under a Paris-proof climate scenario and a comprehensive energy conversion model, this study assesses the projected changes of European VRE supply from the perspective of average production, production variability, spatiotemporal complementarity, and risk of concurrent renewable energy droughts.

For the period 2045–2055, we find a minor reduction in average wind and solar production for most of Europe compared to the period 1990–2010. At the country level, the impact of climate change on average VRE production is rather limited in magnitude (within ±3% for wind and ±2% for solar). The projected mid-term changes in other aspects of VRE supply are also relatively small. This suggests climate-related impacts on European VRE supply are less of a concern if the Paris-proof emission reduction pathway is strictly followed.

Based on spectral analysis, we identify strong seasonal wind-solar complementarities (with an anticorrelation between -0.6 and -0.9) at the cross-regional level. This reduces the demand for seasonal storage but requires coordinated cross-border efforts to develop a pan-European transmission infrastructure.

The risk of concurrent renewable energy droughts between a country and the rest of Europe remains non-negligible, even under the copperplate assumption. Central Western European countries and Poland are most vulnerable to such risk, suggesting the need for the planning of adequate flexibility resources.

## 1. Introduction

To be in line with the Paris Agreement that aims to limit the global mean temperature increase well below 2 °C, the European Union has pledged to achieve economy-wide climate neutrality by 2050 [35]. The energy transition has become a key cornerstone underlying the EU's climate strategy, the *European Green Deal* [34]. This requires developing a power system largely based on variable renewable electricity (VRE) generation technologies that are fuelled by weather resources (e.g., wind and solar). According to recent scenario studies [33,55], the EU should increase the share of VRE in total electricity generation to at least 68% to fulfil its climate ambition. However, the large-scale integration of VRE into the power system inevitably increases its susceptibility to weather and climate conditions. Additional flexibility resources, such as balancing reserves, energy storage, Power-to-X technologies and interconnectors are needed to address the stochastic nature of VRE generation in grid operation [63]. The challenge is further compounded by changing weather patterns due to climate change (e.g., wind profile, solar irradiance, cloud coverage). Not only can changing climate conditions influence the average production and variability of VRE supply, but they may alter the spatiotemporal dependency between VRE assets across location and technology [60,63]. Since the development and operational lifetimes of VRE assets and complementary energy infrastructure span typically from several years to multiple decades, adapting planning and operation of the power system to future climate change becomes crucial for a sustainable and reliable energy supply [88].

* Corresponding author.
*E-mail address:* J.Hu@uu.nl (J. Hu).

https://doi.org/10.1016/j.adapen.2023.100134
Received 7 December 2022; Received in revised form 20 March 2023; Accepted 3 April 2023
Available online 6 April 2023

Based on standard variables simulated from climate models, climate change impacts have been assessed in numerous studies by comparing VRE supply between different future periods and a reference historic period. These impacts, often referred to as "climate signals", are typically measured using statistical measures such as mean, standard deviation and correlation of long time series of VRE output data (10 to 30 years). For instance, the change in mean outputs of one or more VRE technologies has been analysed often at different geographic scales including the world [40], China [39], Japan [82], the Taiwan Strait [17], and several regions within Europe [4,15,21,24,52,53,60,61,71,98,110]. The coefficient of variation or standard deviation (sd) has been applied by Gao et al. [39], Jerez et al. [60], Jerez et al. [61] and Tobin et al. [99] to analyse changes in variability of VRE outputs or output ramps. Next to the univariate statistics of mean and sd characterising individual VRE assets, the climate signals of bivariate metrics measuring the dependence behaviour between VRE assets have also been studied, but to a much lesser extent. For instance, Hou et al. [53] examined climate impacts on the complementarity of daily generation profiles between solar photovoltaics (PV) assets across Europe. Based on an innovative spectral decomposition, Jerez et al. [60] evaluated local wind-solar technological complementarities within various EU regions at multiple timescales spanning from daily to interannual. Both studies employ the Pearson correlation, the most commonly used dependence metric. However, interregional technological dependence or complementarity between wind and solar assets in relation to changing climate conditions have not yet been investigated. Moreover, correlation, which is a linear metric that measures the overall association between two random variables, does not provide insight into the tail behaviour of the joint probability distribution (hereafter referred to as *tail dependence*) [1]. In the context of VRE supply, correlation is unable to capture tail dependence in extreme low or high production events between VRE assets, highlighting the need for alternative dependence metrics in climate impact assessment.

The impact of climate change on VRE supply has been evaluated for different climate scenarios. Within the climate modelling community, climate scenarios are described by representative concentration pathways (RCPs).[1] In the European context, most studies predominantly focus on climate impacts on VRE supply under RCP 8.5 and RCP 4.5 in the long-term future beyond 2070. Directions of projected changes in mean wind and solar outputs as a result of climate change are inconclusive, in part because of varying geographic foci and different levels of detail in energy conversion modelling employed. A detailed review of state-of-the-art literature concerning climate impacts on VRE supply is summarized in Table A1 of the Appendix. Although RCP 8.5 is considered the business-as-usual scenario in some studies [15,52], its realization requires the burning of an unprecedented quantity of coal (37,254 EJ between 2010 and 2100, see, e.g., Riahi et al. [90]) larger than some estimates of recoverable coal reserves [46].[2] By contrast, RCP 4.5 represents an intermediate mitigation scenario, as it lies between emissions reduction efforts prescribed by the current policies and the latest Nationally Determined Contributions[3] Hausfather & Ritchie [113]. As the only scenario consistent with the Paris target and the EU's climate-neutrality ambition, RCP2.6 is highly relevant to understand the implications of strict global climate mitigation for future European VRE supply. Yet it has received little attention so far in the literature except for two studies (with different findings). Yang et al. [110] analysed the change in mean VRE outputs between the near-term (2010–2039) and medium-term (2040–2069) for seven European cities. They found a reduction in solar outputs (−0.01% to −2.29%), but uncertain directions of change (−12.1% to 13.2%) for wind in winter. Based on the ensemble mean of coarse-resolution general circulation models (GCMs), Gernaat et al. [40] found increased and decreased mean outputs for solar and offshore wind respectively in Europe between 2000 and 2050.

To the authors' best knowledge, no studies have evaluated the full implications of RCP2.6 for future European VRE supply beyond the mean outputs before. To fill this knowledge gap, this study characterises and quantifies the climate impact on the availability, variability, and spatiotemporal dependency of VRE supply[4] in Europe based on a set of high-resolution regional climate projections provided by the CORDEX initiative and driven by CMIP5 global circulation models under RCP 2.6 [68,70]. The novelty and scientific contribution can be highlighted for several aspects. First, following a copula-based tail dependence model, we employ the conditional probability of concurrent extremes as a metric to measure the interdependence of low VRE availability between countries. This not only makes it the first study to quantitatively analyse the intercountry risk of compound renewable energy drought ("Dunkelflaute") events, but it also offers new insights into the planning and operation of interconnected energy systems from perspectives of system adequacy and security. Second, we extend the spectral decomposition method of Jerez et al. [60] to assess multi-timescale technological complementarity to cross-regional applications. This enables the identification of cyclic patterns hidden in the original series of VRE outputs and potential spatiotemporal complementarity between VRE assets in different regions. Third, we introduce a comprehensive energy conversion model integrating geospatial data, meteorological reanalysis data, and bias-adjusted climate data to more accurately represent the effect of location-specific topographical features on power production, particularly for wind turbines. Finally, taking into account spatial constraints and land cover classes, we assess the spatially explicit geographic potentials (in terms of maximum installable capacity in MW) for VRE technologies in Europe, excluding unsuitable areas to improve the realism of aggregating VRE generation profiles to country or regional levels.

The geographic scope of Europe in this study is defined as the current 27 Member States (MS) of the European Union[5] plus the United Kingdom (GB), Norway (NO), and Switzerland (CH). Following a bottom-up approach, four commercially mature technologies for VRE generation are explicitly considered, i.e., onshore wind, offshore wind, utility PV, and rooftop PV. We focus on the projected change for VRE generation profiles in the medium-term future period (2045–2055) around 2050, corresponding to a mean temperature increase of about 1.2 °C

[1] RCPs prescribes the evoluation of green house gases (GHGs) concentrations to reach targets that limit radiative forcing increase by 2100 relative to the pre-industrial level. The targets are set at 2.6, 4.5, 6.0 and 8.5 W/m$^2$ to enable a wide span of emission scenarios [74]. At a confidence level between 66%–100%, the global mean temperure increases under RCP2.6, RCP4.5, RCP6.0 and RCP8.5 are respectively 0.3-1.7, 1.1-2.6, 1.4-3.1 and 2.6-4.6 °C [57].

[2] Despite increasing implausibility over time, RCP 8.5 might be arguably justified as the worst-case scenario to compensate for insufficient representation of fat-tailed uncertainties associated with the climate sensitivity in climate modelling (Weitzman, 2011).

[3] Nationally Determined Contributions are non-binding national climate mitigation plans contributing to the Paris target. They are required to be established and updated on a five-year basis by all stipulated parties of the Paris Agreement [102].

[4] In line with other climate impact studies [15,21,24,39,52,53,110], VRE supply under future climate conditions in this study is characterized on the basis of per unit of installed capacity. This means that we do not aim to determine the optimal installed capacity in future energy system, which is a sizing problem, being dependent on future electricity demand and use of storage. A detailed power system model is needed to determine the size of VRE capacity alongside other generation capacity.

[5] They include Austria (AT), Belgium (BE), Bulgaria (BG), Croatia (HR), Cyprus (CY), Czech Republic (CZ), Denmark (DK), Estonia (ES), Finland (FI), France (FR), Germany (DE), Greece (EL), Hungry (HR), Ireland (IR), Italy (IT), Latvia (LV), Lithuania (LT), Luxembourg (LU), Malta (MA), Netherlands (NL), Poland (PL), Portugal (PO), Romania (RO), Slovakia (SK), Slovenia (SI), Spain (ES), and Sweden (SE).

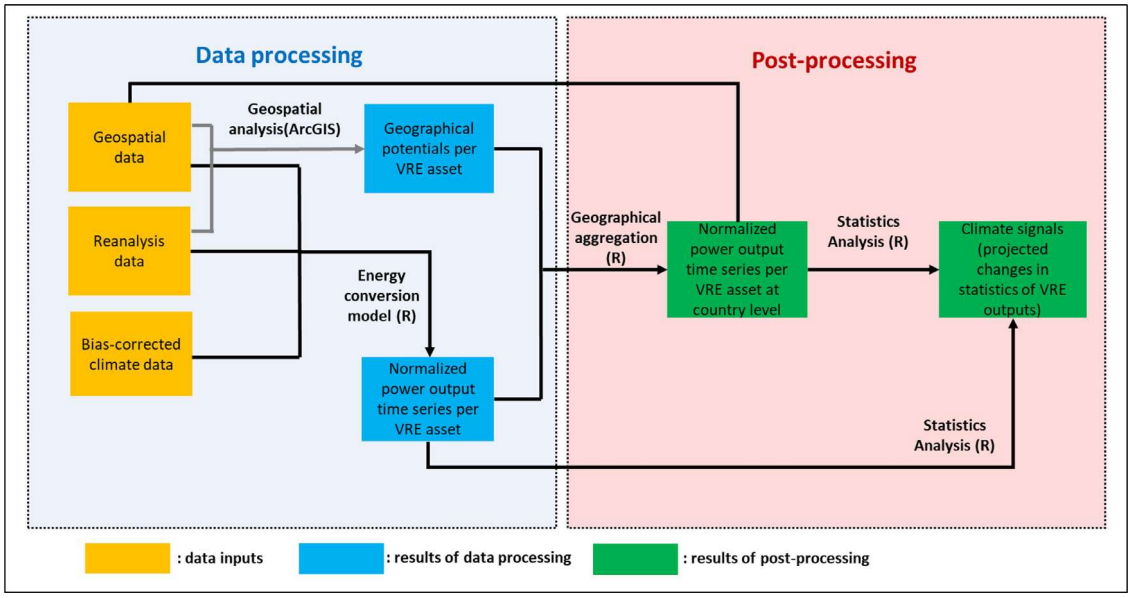


**Fig. 1.** An overview of the research method.

over the European domain compared with 1990–2010.[6] 2050 also represents the year in which the European power system must be fully decarbonized with a high share of VRE. The results of this study can support more informed decision-making and risk management regarding energy policy, power system planning, investment, and financing in renewable projects for policymakers, system planners and operators, utility companies and investors. Beyond the scope of Europe, the method presented in this paper is also repeatable for other regions of the world.

This paper is structured as follows. Section 2 describes the input data and method steps used for data processing and post-processing. This includes an elaboration of the energy conversion model, the geospatial analysis for determining geographic potentials, and the statistical measures employed to characterise VRE supply under historic and projected climate conditions. The results are presented in section 3, followed by a discussion in section 4 regarding the limitations of the study. Finally, concluding remarks are provided in Section 5.

## 2. Data and method

An overview of the method applied to carry out this study is outlined in Fig. 1. The method contains 4 steps that can be divided into a data processing procedure and a post-processing procedure. All steps were performed based on ArcGIS or R. Starting from the input data (Section 2.1), in the data processing procedure we performed a geospatial analysis to characterise the geographic potentials for each VRE asset at a spatially resolved geographic grid over the European domain (Section 2.2). We refer to each VRE technology type located at a specific grid cell as an individual asset. Meanwhile, energy time series (measured by rating factors, which are normalized outputs per unit of installed capacity) for the reference historic and target future periods per VRE asset were determined from bias-adjusted climate data via energy conversion modelling (Section 2.3). The post-processing procedure first aggregated energy time series at grid cell level into country-level series for each considered VRE technology (Section 2.4). Afterwards, country-level climate signals of projected changes in VRE supply based on selected statistics were characterised (Section 2.5).

### 2.1. Input data

The primary data inputs for this study are climate data, meteorological reanalysis data, and geospatial data. This section focuses on climate data and meteorological reanalysis data, while we describe geospatial data and its usage in section 2.2.

- Climate data

We use downscaled high-resolution regional climate model (RCM) data from the CORDEX initiative (www.cordex.org) for the EUR-CORDEX domain. The selected projections all come at 0.11 deg horizontal resolution and follow RCP 2.6. Due to the computational load of the energy conversion model, we were restricted to an ensemble of three projections. Those were selected in a way to cover the spread of the climate signal within the given RCP2.6 as good as possible. We did this by visual inspection of the monthly climate signals and found a clear grouping pattern according to the driving global circulation model (GCM). This is in line with previous studies (e.g. Hawkins & Sutton [47]). Therefore, we chose three projections that all use a different GCM (see Table 1).

We used publicly available data at www.esgf.org which offers a standard set of climate variables (hereafter referred to as “standard climate variables”) for the CORDEX projections. Of those standard variables, three are relevant to the energy conversion of VRE resources, namely surface wind speed at 10 m, surface downward solar radiation and near-surface temperature at 2 m. The variable time series are temporally resolved at 3 hourly.

We followed a standard impact modelling approach in which the climate model data is bias-adjusted before using it as input data for the impact assessment. The regional climate projections were bias-adjusted by the bias-adjustment tool MIdAS [3]. The bias-adjustment aims to adjust the climate model data in a way that they resemble a chosen reference data as closely as possible during a chosen reference period. This procedure thereby makes the usage of climate model data more consistent to the reference data. As reference data, we used the HydroGFD data [2] for temperature, and ERA5 reanalysis data [29] for wind speed at surface and incoming shortwave radiation. The reference data comes at 0.25 deg resolution, and the climate model data at 0.11 deg was interpolated to the 0.25 deg grid of the reference data.

[6] Own calculation based on ensemble mean of climate projections used in this paper, see section 2.1 for details.

**Table 1**
List of climate projections used.

| GCM | RCP | Realization | RCM | Institute | Acronym |
|---|---|---|---|---|---|
| MPI-M-MPI-ESM-LR | RCP2.6 | r1i1p1 | SMHI-RCA4_v1a | SMHI | MPI |
| ICHEC-EC-EARTH | RCP2.6 | r12i1p1 | SMHI-RCA4_v1 | SMHI | ICHEC |
| MOHC–HadGEM2-ES | RCP2.6 | r1i1p1 | KNMI-RACMO22E_v2 | KNMI | MOHC |

**Table 2**
A detailed list of used climate variables and their names in climate data, reanalysis data and this paper.

| Variable name in climate data | Variable name in ERA5 reanalysis data | Variable name in this paper | Relevant to wind energy conversion | Relevant to solar energy conversion |
|---|---|---|---|---|
| Surface speed at 10 m (sfcWind) | 10 m wind speed (wspd) | Wind speed at 10 m (m/s) | Y | Y |
| NA | 100 m windspeed (wspd100m) | Wind speed at 100 m (m/s) | Y | |
| Surface downward solar radiation (rsds) | Surface shortwave radiation downwards (ssrd) | Global horizontal irradiance (W/ $m^2$) | | Y |
| NA | Total sky direct solar radiation at surface (fdir) | Direct component of global horizontal irradiance (W/ $m^2$) | | Y |
| NA | Total sky diffuse solar radiation at surface (fdif) | Diffuse component of global horizontal irradiance (W/ $m^2$) | | Y |
| Near-surface temperature at 2 m (tas) | Temperature at 2 m height (t2m) | Ambient temperature ( °C) | | Y |
| NA | Forecast albedo (fal) | Surface albedo | | Y |

The bias-adjusted data at 3-hourly resolution was further linearly interpolated to 1-hourly resolution in order to meet the energy model's requirements.

- Reanalysis data

Meteorological reanalysis combines the atmospheric circulation model with large numbers of historic observations to deliver a complete, consistent and close-to-reality hindcast of the past weather [29]. As state-of-the-art global meteorological reanalysis, ERA5 reanalysis provides hourly time series data available at 0.25° X 0.25° resolution for the period 1959 to the present. Compared with the bias-adjusted climate data, reanalysis data contains a larger set of variables relevant to the power production of VRE. Information derived from reanalysis data can be directly fed into the energy conversion model. This avoids the use of unnecessary or oversimplified assumptions. Table 2 presents a detailed list of climate variables relevant to the energy conversion of VRE resources and their abbreviations. The same variable can have different names in climate data and reanalysis data. For the sake of convenience, we have unified their names and units in this paper.

### 2.2. Geospatial analysis

Based on a geospatial analysis the geographic potentials for each VRE technology are determined per grid cell. Starting from a 0.25° X 0.25° geographic grid over the territory and exclusive economic zone of Europe, we explicitly exclude areas unavailable for VRE deployment considering a wide range of spatial constraints. The centroid coordinates of each grid cell serve to establish connections with the VRE generation profiles determined from the climate and reanalysis data (see section 2.3). Updated from the authors' previous work [54], a detailed list of spatial constraints and corresponding geospatial data used for each VRE technology is presented in Table 3.

Next, based on the latest CORINE land cover (CLC) inventory [19], the suitability factor (as fraction area per land cover class) determines the areas (in $km^2$) suitable for VRE deployment within the remaining available area. Suitability factors have been used extensively to assess the geographic potentials of VRE technologies, but they vary widely between studies, especially for onshore wind. For instance, they can be as high as 0.9 in Bosch et al. [9], while Zappa and van den Broek [111]; Bruninx [13] assume a uniform low sustainability factor at 0.06 across all land cover classes. In this study, we estimate suitability factors for onshore wind based on Mckenna et al. [73], Hoogwijk et al. [51], Held et al. [48] and Deng et al. [22]. The value is adopted if suitability factors for a certain land cover from more than one source agree with each other. Otherwise, we use a moderate estimator falling within the value range. For offshore wind, a factor of 0.4 is applied to the available ocean area following Hu et al. [54]. The suitability factor for utility PV is mainly based on Hoogwijk [50], where a relatively optimistic value of 0.05 is assigned to areas with sparse vegetation. As for rooftop PV, we conservatively assumed that deployment is exclusively restricted to the roof surface in the urban area, and industrial and commercial units and not on other artificial surfaces. The suitability factors are developed by factoring in the average building footprint[7] per land cover class, the ratio of areas reserved for other usages (assumed at 0.5 according to Bodis et al. [7]), and the composition of roof types. We distinguish two main roof types: flat roof and pitched roof. Based on data sampled from the Stuttgart Region of Germany, it is estimated that 95% and 50% of roof surfaces are pitched for residential and commercial buildings, respectively [92]. The pitch angle of the pitched roof is identically set at 35°, following Zappa and van den Broek [111]. In absence of detailed information, a uniform distribution of the four facets is applied for the orientations of the titled roof surface, but the north-facing roof is excluded from PV installation due to economic considerations.

The suitability factors associated with each land cover class are presented in Table 4.

Finally, the geographic potentials in terms of maximum installable capacity per grid cell are determined based on the specific spacing area (in $km^2$/MW) for each VRE technology. Regional or country-level potentials for each VRE technology can be obtained by summing grid-level potentials within the region or country's border.

Wind turbines are spaced in relation to the rotor diameter (D). Based on 19,221 wind turbine sites clustered to 3800 wind farms in Germany, the average distance between turbines within a single farm is approximately 6D [69]. Therefore, we opted to use a specific spacing area of 6D*6D for both onshore wind and offshore wind in this study. The selection of commercial modules representative of wind installation follows Hu et al. [54]. Three onshore turbine modules and one offshore turbine module from Vestas, the Danish manufacturer, are explicitly considered

[7] Building footprint can be considered as an approximate for the horizontal projected area of the building's roof surface. Detailed building footprint sampled from the Netherlands and the United Kingdom is extracted from Zappa and van den Broek [111].

**Table 3**
Spatial constraints for the exclusion of areas unavailable for the development of four VRE technologies.

| Spatial constraints for each VRE technology | Data sources | Resolution of data (NA in case of shapefile) | Onshore wind | Offshore wind | Utility PV | Rooftop PV |
|---|---|---|---|---|---|---|
| Territory ($km^2$) | Nomenclature of Territorial Unis for Statistics (NUTS) Maps 2016 [36]; Union of the ESRI Country shapefile and the Exclusive Economic Zones (version 3) [38] | NA | Administrative terrestrial area | Economical exclusive zone | Administrative terrestrial area | Administrative terrestrial area |
| Distance to shore (km) | NA | NA | NA | 10–185<br>A minimum distance to shore at ~10 km is set to restrict visibility and environmental impacts of offshore wind farms. The maximum distance to shore is limited to 185 km for cost consideration [32] | NA | NA |
| Depth (m) | General bathymetric chart of the oceans (GEBCO)_2020 [11] | 0.004° (0.25 arcmin) | NA | ≤ 60<br>Only offshore wind turbines with bottom fixed foundations (no floating) are considered. They usually suit at a water depth below 60 m [84] | NA | NA |
| Commercial vessel identity and location information | Recent pace of change in human impact on the world's ocean[9] [45] | 0.1°<br>(6 arcmin) | NA | ≤1500. If the grid cell includes more than 1500 vessel locations, it is considered as vessel-intensive areas to be excluded from the available area for offshore wind farms. | NA | NA |
| Oil rigs | Global Gas Flaring Estimates 2006 [78]; Global DMSP-OLS Nighttime Lights Time Series 1992 - 2013 (Version 4) [79] | 0.008°<br>(0.5 arcmin) | NA | Full exclusion | NA | NA |
| Submarine communications cable | Greg's Cable Map of undersea cable initiatives [72] | NA | NA | 1 $km^2$ buffering from both sides of the cable [9] | NA | NA |
| Protected areas ($km^2$) | Protected Planet: The World Database on Protected Areas (WDPA) [101] | NA | Terrestrial protected areas | Terrestrial & maritime protected areas | Terrestrial protected areas | Terrestrial protected areas |
| Permafrost (%) | Global Permafrost Zonation Index Map [44] | 0.008°<br>(0.5 arcmin) | ≤0.1 | NA | ≤0.01 | ≤0.01 |
| Elevation (m) | Digital Elevation - Global 30 Arc-Second Elevation (GTOPO30) [103] | 0.05°<br>(30 arcmin) | <=2500<br>Following Eurek et al. [32], elevation above 2500 m is considered as too high for onshore wind development due to a substantial reduction of wind power density associated with air density losses. | NA | NA | NA |
| Slope (degree) | Calculated based on Elevation | 0.05°<br>(30 arcmin) | <11.31 (or 20%) [32] | NA | <4 (0r 6.99%)<br>(Sun et al., 2013) | NA |
| Land cover | GlobCover 2009 V2.3 Global Land Cover Map [8]; Corine Land Cover Inventory (CLC) 2018 [19] | 0.003°<br>(1.67 arcmin) for GlobCover 2009 V2.3; 100 m for CLC2018 | Depending on the suitability factor per land cover type | NA | Depending on the suitability factor per land cover type | Depending on suitable rooftop areas in the built-up area |

Source: Updated based on Hu et al. [54].

[9] Data under the name "raw_2013_shipping_mol.zip" accessed via https://knb.ecoinformatics.org/view/resource_map_doi:10.5063/F1NZ85ZN.

**Table 4**
Sustainability factors for different CLC land cover classes.

| CLC land cover Class | 1st Sub-Class | 2nd Sub-Class | CLC Code | Suitability factor | | | | |
|---|---|---|---|---|---|---|---|---|
| | | | | Onshore wind | Offshore wind | Utility PV | Rooftop PV | |
| | | | | | | | *Pitched roof* | *Flat roof* |
| Artificial surfaces | Urban fabric | Continuous urban fabric | 111 | 0 | 0 | 0 | 0.119 | 0.007 |
| | | Discontinuous urban fabric | 112 | 0 | 0 | 0 | 0.067 | 0.004 |
| | Industrial, commercial and transport units | Industrial or commercial units | 121 | 0 | 0 | 0 | 0.041 | 0.045 |
| | | Road and rail networks and associated land | 122 | 0 | 0 | 0 | 0 | 0 |
| | | Port areas | 123 | 0 | 0 | 0 | 0 | 0 |
| | | Airports | 124 | 0 | 0 | 0 | 0 | 0 |
| | Mine, dump and construction sites | Mineral extraction sites | 131 | 0 | 0 | 0 | 0 | 0 |
| | | Dump sites | 132 | 0 | 0 | 0 | 0 | 0 |
| | | Construction sites | 133 | 0 | 0 | 0 | 0 | 0 |
| | Artificial, non-agricultural vegetated areas | Green urban areas | 141 | 0 | 0 | 0 | 0 | 0 |
| | | Sport and leisure facilities | 142 | 0 | 0 | 0 | 0 | 0 |
| | Arable land | Non-irrigated arable land | 211 | 0.2 | 0 | 0.01 | 0 | 0 |
| | | Permanently irrigated land | 212 | 0 | 0 | 0 | 0 | 0 |
| | | Rice fields | 213 | 0 | 0 | 0 | 0 | 0 |
| | Permanent crops | Vineyards | 221 | 0.1 | 0 | 0.01 | 0 | 0 |
| | | Fruit trees and berry plantations | 222 | 0.1 | 0 | 0.01 | 0 | 0 |
| | | Olive groves | 223 | 0.1 | 0 | 0.01 | 0 | 0 |
| | Pastures | Pastures | 231 | 0.2 | 0 | 0.01 | 0 | 0 |
| | Heterogeneous agricultural areas | Annual crops associated with permanent crops | 241 | 0.2 | 0 | 0.01 | 0 | 0 |
| | | Complex cultivation patterns | 242 | 0.2 | 0 | 0.01 | 0 | 0 |
| | | Agricultural land with significant natural vegetation | 243 | 0.2 | 0 | 0.01 | 0 | 0 |
| | | Agro-forestry areas | 244 | 0.1 | 0 | 0 | 0 | 0 |
| Forest and semi natural areas | Forests | Broad-leaved forest | 311 | 0 | 0 | 0 | 0 | 0 |
| | | Coniferous forest | 312 | 0 | 0 | 0 | 0 | 0 |
| | | Mixed forest | 313 | 0 | 0 | 0 | 0 | 0 |
| | Scrub and/or herbaceous vegetation associations | Natural grasslands | 321 | 0.2 | 0 | 0.01 | 0 | 0 |
| | | Moors and heathland | 322 | 0.1 | 0 | 0.01 | 0 | 0 |
| | | Sclerophyllous vegetation | 323 | 0.1 | 0 | 0.01 | 0 | 0 |
| | | Transitional woodland-shrub | 324 | 0 | 0 | 0 | 0 | 0 |
| | Open spaces with little or no vegetation | Beaches, dunes, sands | 331 | 0 | 0 | 0 | 0 | 0 |
| | | Bare rocks | 332 | 0 | 0 | 0 | 0 | 0 |
| | | Sparsely vegetated areas | 333 | 0.5 | 0 | 0.05 | 0 | 0 |
| | | Burnt areas | 334 | 0 | 0 | 0 | 0 | 0 |
| | | Glaciers and perpetual snow | 335 | 0 | 0 | 0 | 0 | 0 |
| Wetlands | Inland wetlands | Inland marshes | 411 | 0 | 0 | 0 | 0 | 0 |
| | | Peat bogs | 412 | 0 | 0 | 0 | 0 | 0 |
| | Maritime wetlands | Salt marshes | 421 | 0 | 0 | 0 | 0 | 0 |
| | | Salines | 422 | 0 | 0 | 0 | 0 | 0 |
| | | Intertidal flats | 423 | 0 | 0 | 0 | 0 | 0 |
| Water bodies | Inland waters | Water courses | 511 | 0 | 0 | 0 | 0 | 0 |
| | | Water bodies | 512 | 0 | 0 | 0 | 0 | 0 |
| | Marine waters | Coastal lagoons | 521 | 0 | 0 | 0 | 0 | 0 |
| | | Estuaries | 522 | 0 | 0 | 0 | 0 | 0 |
| | | Sea and ocean | 523 | 0 | 0.4 | 0 | 0 | 0 |

Source: compiled based on Copernicus (2018); Bosch et al. [9]; Zappa and van den Broek [111]; Brunnix et al. [13]; Mckenna et al. [73]; Hoogwijk [50]; Held et al. [48]; Deng et al. [22]; Bodis et al. [7]; Sliz-Szkliniarz [92].

(see Table 4 for detailed technical specifications including the rotor diameter).

The Sanyo HIP-225HDE1 module is adopted for the installation of both utility PV and rooftop PV. It has a rated capacity of 0.225 $kW_p$ corresponding to a panel surface area of 1.39 $m^2$ [85]. The specific spacing area for PV depends on the mounting method. For rooftop PV installed on a flat roof or utility PV mounted on close-to-flat ground (slope ≤ 4 °), the PV panels are mounted at empirical PV angles to maximize energy yields. In this case, the panel azimuth angle ($Z_p$) is set at 180°, i.e., facing true south. Based on rule-of-thumb, the empirical panel tilt angle ($\beta$) in Northern hemisphere is a function of the local latitude ($L$) [18]:

$$\beta = 0.764L + 2.14°, \ for \ L \leq 65° \tag{1}$$

$$\beta = 0.224L + 33.65°, \ for \ L > 65° \tag{2}$$

The specific spacing area is a function of panel angles and solar angles under a reference condition to avoid self-shading [20]:

$$S_{PV} = A_{PV}\left(\cos\beta + \frac{\sin\beta}{\tan\alpha_{ref}}\cos\left(Z_{s,ref} - Z_p\right)\right) \tag{3}$$

Where $A_{PV}$: Specific PV panel area;

$\beta$ and $Z_p$: panel tilt angle and azimuth angle;
$\alpha_{ref}$ and $Z_{s,ref}$: solar altitude angle and azimuth angle under the reference condition

The third lowest hourly solar attitude angle on December 21st (winter solstice) is set as the reference condition for low latitude areas ($L$ <60°) [20], while for high latitude areas ($L \geq 60°$) November 1st is used instead to avoid negative altitude angle. The mounting of rooftop PV on the pitched roof surface is constrained by the pitch angle and orientation of the roof. We exclude the possibility of tilted mounting. This means that the PV system must be installed parallel to the roof surface. In this case, the specific spacing area equals the specific panel area.

### 2.3. Energy conversion model

#### 2.3.1. Wind

Wind energy conversion is mainly based on power curves of representative commercial wind turbines, but additional adjustments are integrated in the model to consider effects of local elevation, propagation of wind speed and wake losses. The same conversion model is applied for both onshore and offshore wind in this study, except for that the power curve for offshore wind at sea level does not need to be adjusted for elevation. This follows a five-step approach.

First, we extrapolate the climate variables of wind speed at a reference height (10 m) to wind speed at turbine hub height. Following van Zuijlen et al. [104], we assume the hub height for onshore and offshore wind are 150 m and 100 m respectively. The extrapolation is based on the power law profile:

$$v_z = v_{ref}\left(\frac{z}{z_{ref}}\right)^{\alpha} \tag{4}$$

where $v_z$ and $v_{ref}$ are wind speeds corresponding to the turbine height ($z$) and reference height ($z_{ref}$); $\alpha$ is the shear exponent.

The shear exponent is not readily available for either reanalysis data or climate data. However, since the reanalysis data provides two variables of wind speed at 10 m and 100 m, regression is used to derive grid cell-specific exponents. The same set of exponents is applied to the climate data, which contains only one wind variable, i.e. surface wind speed at 10 m. Compared with most studies simply assuming two uniform exponents for land (0.143) and sea (0.11), this avoids unnecessary bias in estimating wind speed at turbine height.

Secondly, we characterise wind class per grid cell and assign suitable turbine modules based on the IEC's classification (see Table 5). In this study, we select 3 onshore modules and 1 offshore module from the Danish manufacturer Vestas. The power curves of the 4 turbine modules are presented in Fig. 2, which describe the relationship between wind speed and the corresponding wind power rating factor at standard test conditions.

In the third step, we determine the elevation-adjusted power curve per wind site. The kinetic power ($P_{wind}$) extracted by the wind turbine is theoretically proportional to air density ($\rho_h$):

$$P_{wind} = 0.5C_p\rho_h A v_z^3 \tag{5}$$

Where $A$ is the area swept by the turbine blades, $C_p$ is the power coefficient and $P_{rated}$ is the rated power.

Hence, the impact of elevation associated with wind sites above sea level on air density should be considered when using the power curve to extract the rating factor. The relationship between elevation ($h$) and air density simply reads:

$$\rho_h = \rho_0 - \gamma h \tag{6}$$

where $\rho_0 = 1.225 kg/m^3$ is the air density at zero elevation and $\gamma = 1.194 \cdot 10^{-4}$ $kg/m^2$ is a proportionality constant. The proportional relationship between power and air density in formula (5) can be used to calculate the rating factor corrected for air density along every wind speed of the original power curve (e.g. Hu et al. [54]), but it is only suitable for stall-regulated wind turbines [97]. For modern pitch-regulated turbines considered in this study, we follow the approach of Eurek et al. [32]to reconstruct the power curve adjusted to air density. It calculates the equivalent wind speed for each rating factor along the original power curve via formula (7)

$$v_h = v_z\left(\rho_h/\rho_z\right)^{-1/m} \tag{7}$$

The exponent $m$ is a function of wind speed, according to Svenningsen [97]. It is constant at 3 until the wind speed reaches 7.5 m/s, linearly decreases to 1.5 until 12.5 m/s and remains constant afterwards.

Next, we develop the multi-turbine power curve from the elevation-adjusted single turbine power curve for each grid cell. The multi-turbine power curve factors into the spatial propagation of wind speed within a specific site under the same wind regime. Because generation across multiple turbines is not fully synchronous, the aggregated outputs are smoothed out to a certain extent. Assuming the instantaneous wind speed follows a Gaussian distribution within a specific site, most existing studies (Norgaard and Holttinen [80]; Gibescu et al. [42]; Staffell and Pfenninger [95]) apply a Gaussian filter to the single turbine power curve to develop the multi-turbine curve. However, the method to determine sd of the Gaussian filter diverges between studies. The method to determine the Gaussian filter sd is adapted from Gibescu et al. [42] in this study, because it has several advantages over other methods. It does not require assumptions about turbulence intensity or high-frequency wind speed data to calculate it. Furthermore, it takes site-specific dimensional characteristics into account, enabling the determination of Gaussian filters for each grid cell.

The sd of the Gaussian filter ($\sigma_s$) for a specific wind site at grid cell level can be calculated according to formulas (8)-(10)

$$\sigma_G = \sigma_t\sqrt{0.5\left(1 - e^{-\bar{d}/D_{decay}}\right)} \tag{8}$$

$$\bar{d} = \frac{d_{max} + 2d_{min}}{3} \tag{9}$$

$$d_{max} = 2\sqrt{\frac{A_{wind}}{\pi}} \tag{10}$$

Where,

$\sigma_t$: sd associated with site-specific wind speed time series;
$\bar{d}$: average distance between two random wind turbines within the same site;

**Table 5**
Key characteristics of four Vestas turbine modules corresponding to the IEC's wind site classification.

| IEC's wind turbine classification according to average wind speed at turbine height | Usage | Representative commercial turbine module | Rated capacity (MW) | Rotor diameter (m) | Specific power (W/m) | Cut-in speed (m/s) | Rated speed (m/s) | Cut-off speed (m/s) |
|---|---|---|---|---|---|---|---|---|
| Class I: >8.5 m/s | Onshore | Vestas 105–3.3 | 3.3 | 105 | 381.8 | 3 | 13 | 25 |
| Class II: 7.5–8.5 m/s | Onshore | Vestas 117–3.3 | 3.3 | 117 | 306.9 | 3 | 13 | 25 |
| Class III: 6 - 7.5 m/s | Onshore | Vestas 126–3.3 | 3.3 | 126 | 264.7 | 3 | 12 | 22.5 |
| Class IV: <6 m/s | NA | | | | | | | |
| Class S: User-defined (Offshore) | Offshore | Vestas 164–8.0 | 8 | 164 | 378.7 | 4 | 13 | 25 |

Sources: IEC [56]; Wind turbine models.com [106–109].

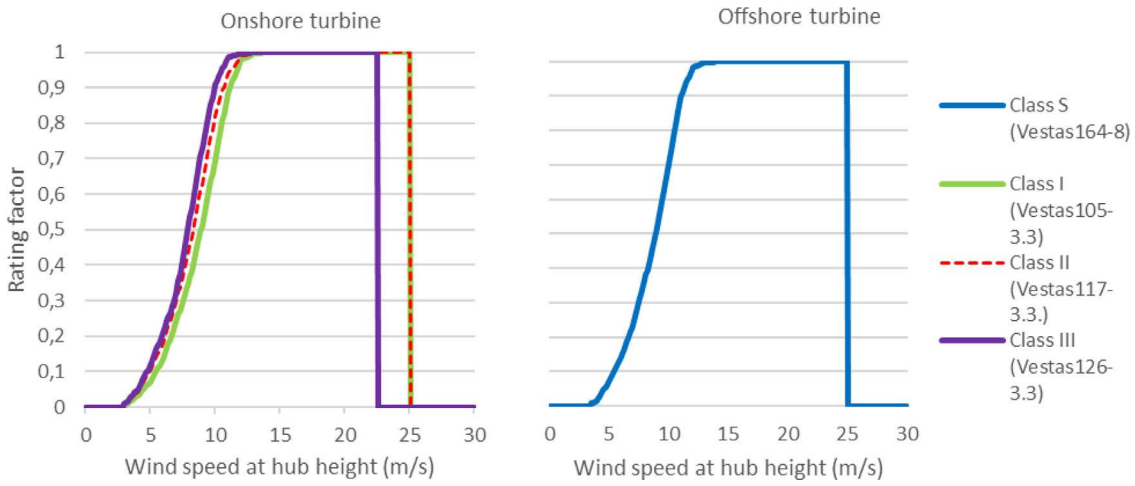


**Fig. 2.** Power curves for four Vestas wind turbine modules.

$D_{decay}$: characteristic distance or decay parameter characterising the exponentially decaying relationship between correlation in wind speeds and the distance, which is 723 km for Europe [43];
$d_{max}$: the maximum distance between two wind turbines within the same site;
$d_{min}$: the minimum distance between two wind turbines within the same site, which is array spacing distance (6D) between two adjacent turbines;
$A_{wind}$: available area for wind development within a grid cell-based wind site.

For illustrative purposes, Fig. 3 presents the original single turbine power curve at sea level for a Class III wind turbine, the air-density adjusted power curve at 1200 m as well as the multi-turbine power curve.

The last step considers efficiency losses after determining the hourly rating factor time series per wind site using the multi-turbine power curve. We distinguish efficiency losses between wake losses and other losses. Wake losses describe the effect of wind speed reduction for downwind turbines located at the shaded area of upwind turbines, which is a function of the array spacing of the wind farm. While most studies assume a fixed ratio of wake losses, we consider wake losses as a function of wind speed based on Knorr [69]. Fig. 4 plots the impact of mean wake losses on turbine efficiency in relation to wind speed for the Knorr dataset containing 3800 German wind farms. For comparison, the efficiency curve associated with the Dena dataset [69], including 12 specific German wind farms, is also presented. It is deemed that the Knorr dataset is more universally applicable as the sample size is much larger. Compared with an 8% fixed rate of wake losses often assumed in Zappa and van den Broek [111], the maximum wake losses based on the Knorr dataset is less than 4%. For other losses (e.g., mechanical and electrical conversion losses), a 5% fixed ratio is assumed to be consistent with other studies [111].

### 2.3.2. Solar PV

The energy conversion for both utility PV and rooftop PV follows the same four-step method.

Firstly, we determine the solar angles per grid cell based on the local geographic coordinates (longitude and/or latitude) and the Coordinated Universal Time (UTC) timestamp. The timestamp is set at the mid-point of each hour in the time series. The most important solar angles are the solar altitude angle and azimuth angle. The readers are referred to Hu et al. [54] and Kalogirou [64] for the detailed formulas used to perform the calculation.

Secondly, a decomposition model is used to determine the global horizontal irradiance ($I_h$) into the direct ($I_{dir,h}$) and diffuse ($I_{dif,h}$) components. The fraction ($df$) of the diffuse component in global horizontal irradiance follows a function conditional on the clearness index ($k$) [30]:

$$k = I_h / I_o \tag{11}$$

$$df = \frac{I_{dif,h}}{I_{dir,h}} = \begin{cases} 1 - 0.09k \ \ for\ k \le 0.22 \\ 0.9511 - 0.1604k + 4.388k^2 - 16.638k^3 + \ 12.336k^4 \\ \quad for\ 0.22 \ < k \le 0.8 \\ 0.165 \ for\ k > 0.8 \end{cases} \tag{12}$$

where k, $I_h$, $I_o$ are the clearness index, global horizontal irradiance and extraterrestrial horizontal irradiance.

For reanalysis data, the direct and diffuse components of global horizontal irradiance are readily available, while for climate data, only

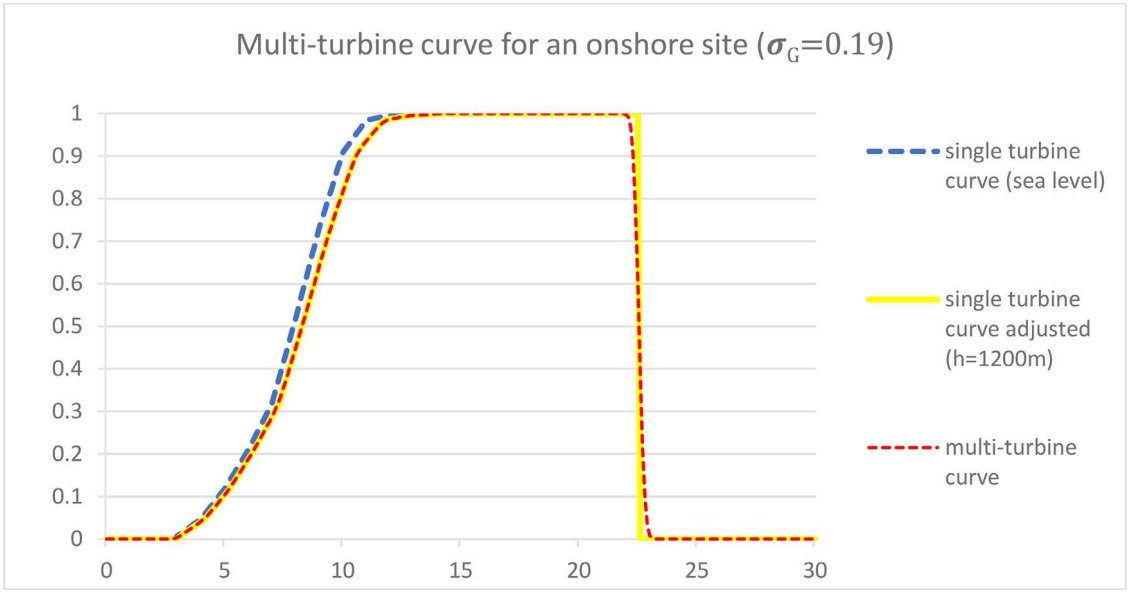


**Fig. 3.** Illustration of a multi-turbine power curve for onshore wind site.

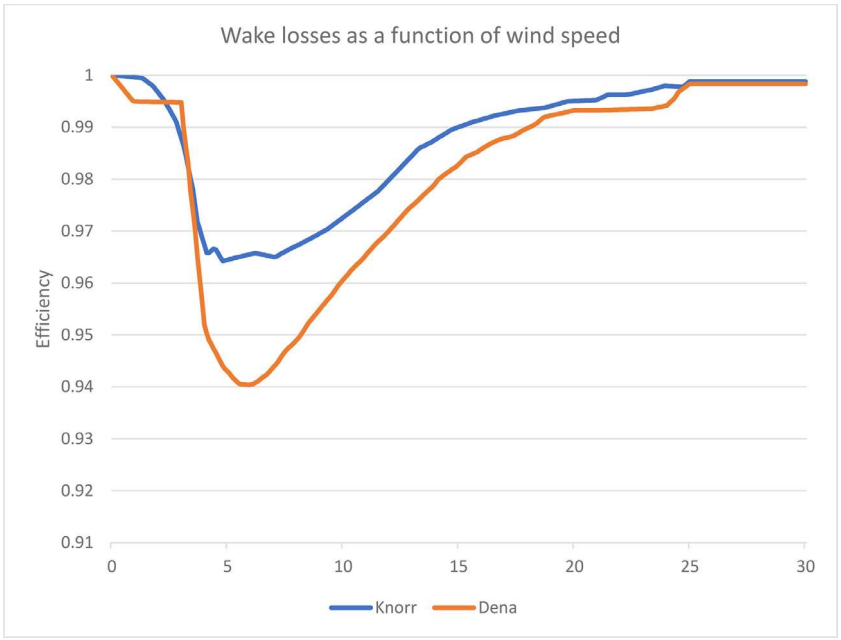


**Fig. 4.** Illustration of wake losses as a function of wind speed. Source: Based on Knorr [69].

global horizontal irradiance is given. Therefore, we need to estimate the extraterrestrial horizontal irradiance [28]:

$$I_0 = \frac{12 \cdot 3.6}{\pi} I_{sc} E_0 \left( (\sin L \cos \delta)(\sin H_2 - \sin H_1) + \frac{\pi (H_2 - H_1)}{180} (\sin L \sin \delta) \right) \tag{13}$$

$$E_0 = 1 + 0.0033 \cos t \left( \frac{2\pi n}{365} \right) \tag{14}$$

Where $I_{sc}$ is solar constant (1367 W/m$^2$); $E_0$ is eccentricity correction factor; $\delta$ is declination angle; $L$ is local latitude; $H_2$ and $H_1$ are the hour angle at the start and end of the time interval of UTC.

Thirdly, we use a transposition model to determine the plane of the array (POA) irradiance, which is total irradiance received by a PV panel based on solar angles and panel angles (see section 2.2).

The hourly POA irradiance ($I_p$) consists of direct ($I_{dir,p}$), diffuse ($I_{dif,p}$) and reflection ($I_{r,p}$) components:

$$I_p = I_{dir,p} + I_{dif,p} + I_{r,p} \tag{15}$$

Depending on the panel tilt angle ($\beta$) and azimuth angle ($Z_p$), the three irradiance components can be determined via (Gulin et al., 2013):

$$I_{dir,p} = \frac{I_{dir,h} \cos(\theta)}{\cos(90 - \alpha)} \tag{16}$$

$$\cos(\theta) = \sin(\alpha)\cos(\beta) + \cos(\alpha)\sin(\beta)\cos\left(Z_p - - Z_s\right) \tag{17}$$

$$I_{dif,p} = \frac{1 + \cos\beta}{2} I_{dif,h} \tag{18}$$

$$I_{r,p} = \frac{1 - \cos\beta}{2} \left( I_{dir,h} + I_{dif,h} \right) Alb \tag{19}$$

**Table 6**
Mount configurations and corresponding heat transfer coefficients.

| PV technology | Mount type | Mount | $a$ | $b$ | $\Delta T_{cond}$ (°C) |
|---|---|---|---|---|---|
| Utility PV | Glass-cell-glass | Open rack | −3.47 | −0.0594 | 3 |
| Rooftop PV | Glass-cell-glass | Close roof | −2.98 | −0.0471 | 1 |

Source: [25].

where $\alpha$ and $Z_s$ are solar altitude angle and azimuth angle; $\theta$ is incidence angle; Alb is surface albedo.

Lastly, we determine hourly RF of PV, considering efficiency losses due to non-standard test conditions and the cell operating temperature [25].

$$RF = \left(\frac{I_p}{I_{STC}}\right)\left[1-\varepsilon\left(T_{NOCT}-T_{cell}\right)\right]PR \tag{20}$$

$$T_{cell} = T_{back} + \left(\frac{I_p}{I_{STC}}\right)\Delta T_{cond} \tag{21}$$

$$T_{back} = I_p \exp^{(a+b*v_{2m})} + T \tag{22}$$

Where $I_{STC}$ (1000 W/m$^2$) is solar irradiance at standard test conditions (STC); PR is the performance ratio to consider PV system losses, e.g., due to inverter losses, shading and dust. The PR is assumed to be 0.9 in this study, which is the upper bound of today's typical PV modules in Germany [87]; $T_{cell}$ and $T_{NOCT}$ (44 °C) are respectively cell operating temperature and nominal operating cell temperature; $\epsilon$ is the temperature coefficient of power indicating the dependence of PV power on cell temperature, which is −0.003 for the selected Sanyo HIP-225HDE1PV module; $T_{back}$ is module back surface temperature, which is a function of empirical coefficients for convective heat transfer ($b$), ambient wind speed at 2 m ($v_{2m}$) and ambient temperature ($T$); $\Delta T_{cond}$ is conduction-induced temperature change. $\Delta T_{cond}$, $a$ and $b$ depend on the materials and mount configurations of the PV module. The assumed mount configurations for both utility PV and rooftop PV and corresponding empirical heat transfer coefficients in this study are provided in Table 6.

### 2.4. Geographic aggregation

To avoid collinearity, utility PV and rooftop PV are aggregated into a single "PV" asset in each grid cell based on the geographic potentials of both technologies. Similarly, grid cell based VRE asset profiles are also aggregated at the country or regional level for different analysis purposes. We divide the 30 European countries into nine regions: Alpine (AT, CH, IT, MT, SI), Baltic (EE, LT, LV), East (CZ, HU, PL, SK), France, Iberia (ES, PT), Isles (GB, IE), Nordic (DK, FI, NO, SE), Southeast (BG, CY, EL, HR, RO) and West (BE, DE, LU, NL). Where it is applicable, the country or regional level VRE assets are further aggregated across technology types. For instance, onshore and offshore wind assets per country are aggregated into a wind asset, whilst wind and solar assets can be aggregated into one asset as well to represent the underlying country-wide technology mix. The aggregation is based on the share of geographic potentials per technology in total potentials.

### 2.5. Statistical analysis

#### 2.5.1. Statistics description

The statistical analysis characterises the rating factor time series per VRE technology for the reference historic and target future periods and to quantify the climate signals, i.e. the mean, sd, (Pearson) correlation, and conditional probability of concurrent extreme low production events. Based on spectral analysis, we decompose the original rating factor time series of VRE assets into time series components at multiple timescales ranging from hourly to yearly (see section 2.5.2). The sd and correlation are also calculated for each component timescale.

Being univariate statistics, the mean and sd of the rating factor time series respectively measure the average output (which is also referred to as the capacity factor) and output variability for each VRE asset. By contrast, correlation is a bivariate measure describing the overall linear dependence structure between random variables. In the context of VRE generation, correlation (or anticorrelation being the inverse of correlation) has been widely used to gauge the temporal complementarity between pairwise VRE assets. This is because (mathematically), a high negative correlation implies a large potential to reduce the total variance of the combined outputs of the underlying assets. However, correlation cannot capture the tail dependence between pairwise VRE assets, which is the comovement of extreme VRE production events [1]. To illustrate this, we plot the probability heat map of the quantile interval of wind generation in Germany conditional on the quantile interval of wind generation in France in Fig. 5.

Conditional on most quantile intervals of French wind generation, there is a considerable spread of the probability distribution of German wind generation. However, at the bottom and top 0.1 quantile intervals, the distribution of German wind generation is heavily skewed towards the lower and upper tail. This suggests a strong degree of tail dependence. In this study, the tail dependence between VRE assets is measured by the conditional probability of concurrent extreme low production events (see section 2.5.3).

The four statistics are characterised for all climate simulations named after the three GCMs. The capacity factor (CF) is characterised for assets at grid cell level as well as at aggregated country level. The other three statistics are characterised for assets at aggregated country or regional level to avoid computational costs.

We only present and analyse the intermodel ensemble mean of the characterised statistics in the Results section for dimension reduction and best visualization of figures. This is in line with other studies (e.g. Gernaat et al. [40]; Miller and Keith [77]). The ensemble mean enables the quantification of the expected value or best estimate of the climate signal, but it does not convey information regarding the uncertainty and robustness of the climate signal. The latter can be captured by the analysis of the ensemble spread, which is beyond the scope of this study.

#### 2.5.2. Decomposition of VRE outputs at multiple time scales

The decomposition of time series into components at different multiple time scales/temporal frequencies usually requires spectral analysis such as Fourier or Wavelet, which is computationally non-trivial. Here we use a simple method adapted from Jerez et al. [60]. One main difference between Jerez et al. [60] and this analysis lies in the temporal resolution of the original time series, which is daily in Jerez et al. [60] but hourly in this study (measured by rating factors). If we denote the original hourly rating factor series as $RF_{y,m,d,h}$ with subscripts $y$, $m$, $d$ and $h$ indicating the specific year, month, day and hour of the time stamp:

$$RF_{y,m,d,h} = \overline{RF_y} + \delta_{y,m} + \delta_{y,m,d} + \delta_{y,m,d,h} \tag{23}$$

$$\delta_{y,m} = \overline{RF_{y,m}} - \overline{RF_y} \tag{24}$$

$$\delta_{y,m,d} = \overline{RF_{y,m,d}} - \overline{RF_{y,m}} \tag{25}$$

$$\delta_{y,m,d,h} = RF_{y,m,d,h} - \overline{RF_{y,m,d}} \tag{26}$$

where $\overline{RF_y}$, $\overline{RF_{y,m}}$ and $\overline{RF_{y,m,d}}$ are yearly, monthly and daily mean of the hourly rating factor series, $\delta_{y,m}$, $\delta_{y,m,d}$ and $\delta_{y,m,d,h}$ are intra-annual monthly deviations concerning the annual mean rating factor, intra-month deviations concerning the monthly mean rating factor, and intra-day hourly deviations concerning the daily mean rating factor.

$\delta_{y,m}$, $\delta_{y,m,d}$ and $\delta_{y,m,d,h}$ can be further decomposed into

$$\delta_{y,m} = \overline{\delta_m} + \left(\delta_{y,m} - \overline{\delta_m}\right) \tag{27}$$

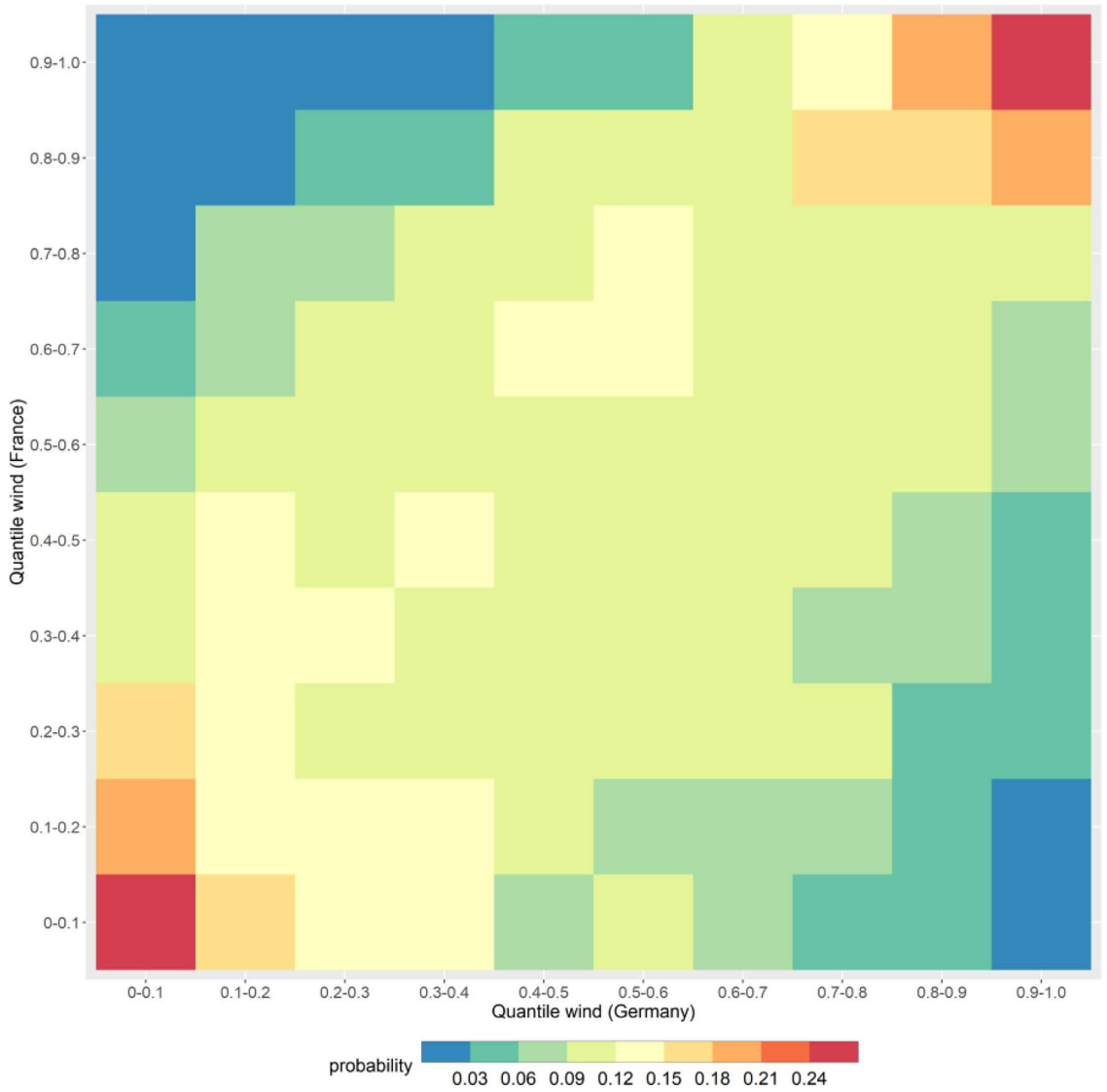


**Fig. 5.** Probability heat map of quantile interval of wind generation in Germany conditional on the quantile interval of wind generation in France.

$$\delta_{y,m,d} = \overline{\delta_{m.d}} + \left(\delta_{y,m,d} - \overline{\delta_{m.d}}\right) \tag{28}$$

$$\delta_{y,m,d,h} = \overline{\delta_{m.d,h}} + \left(\delta_{y,m,d,h} - \overline{\delta_{m.d,h}}\right) \tag{29}$$

Where $\overline{\delta_m}$, $\overline{\delta_{m.d}}$ and $\overline{\delta_{m.d,h}}$ are the interannual monthly mean of $\delta_{y,m}$, interannual daily mean of $\delta_{y,m,d}$, and interannual hourly mean of $\delta_{y,m,d,h}$.

We can rewrite formula (23) as:

$$RF_{y,m,d,h} = \overline{RF_y} + \overline{\delta_m} + \left(\delta_{y,m} - \overline{\delta_m}\right) + \overline{\delta_{m.d}} + \left(\delta_{y,m,d} - \overline{\delta_{m.d}}\right) + \overline{\delta_{m.d,h}} + \left(\delta_{y,m,d,h} - \overline{\delta_{m.d,h}}\right) \tag{30}$$

Hence, formula (30) in essence decomposes the original whole hourly series (WHS) into the sum of the year-to-year (Y2Y) noise term denoted as $RF_y$, the intra-annual monthly (MIA) cycle denoted as $\overline{\delta_m}$, the month-to-month noise term (M2M) denoted as $(\delta_{y,m} - \overline{\delta_m})$, the intra-month daily (DIM) cycle denoted as $\overline{\delta_{m.d}}$, the day-to-day noise term (D2D) denoted as $(\delta_{y,m,d} - \overline{\delta_{m.d}})$, the intra-daily (HID) cycle denoted as $\overline{\delta_{m.d,h}}$, and the hour-to-hour noise (H2H) denoted as $(\delta_{y,m,d,h} - \overline{\delta_{m.d,h}})$:

$$\text{WHS} = \text{Y2Y} + \text{MIA} + \text{M2M} + \text{DIM} + \text{D2D} + \text{HID} + \text{H2D} \tag{31}$$

For illustration purposes, the WHS series for wind and solar assets aggregated at the EU level is decomposed into information components at different time scales in Fig. 6. Decomposition is helpful to identify cyclic patterns hidden in the original series and potential spatiotemporal complementarity between assets.

Since the decomposed components are independent of each other, the variance (VAR) of the WHS can also be decomposed into the sum of VAR associated with different components:

$$VAR_{WHS} = VAR_{Y2Y} + VAR_{MIA} + VAR_{M2M} + VAR_{DIM} + VAR_{D2D} + VAR_{HID} + VAR_{H2H} \tag{32}$$

For each component, we calculate the normalized standard deviation for country-level wind and solar assets to identify the timescales which dominate hourly output variability of the underlying assets. The normalization is based on the mean of the original RF series. Furthermore, the cross-correlation between wind and solar assets aggregated at the regional level is also quantified for each timescale.

### 2.5.3. Tail dependence

Tail dependence describes the comovement of extreme value events in the tail of the distributions of random variables. Generation profiles of two or more VRE assets can exhibit tail dependence in the lower and/or

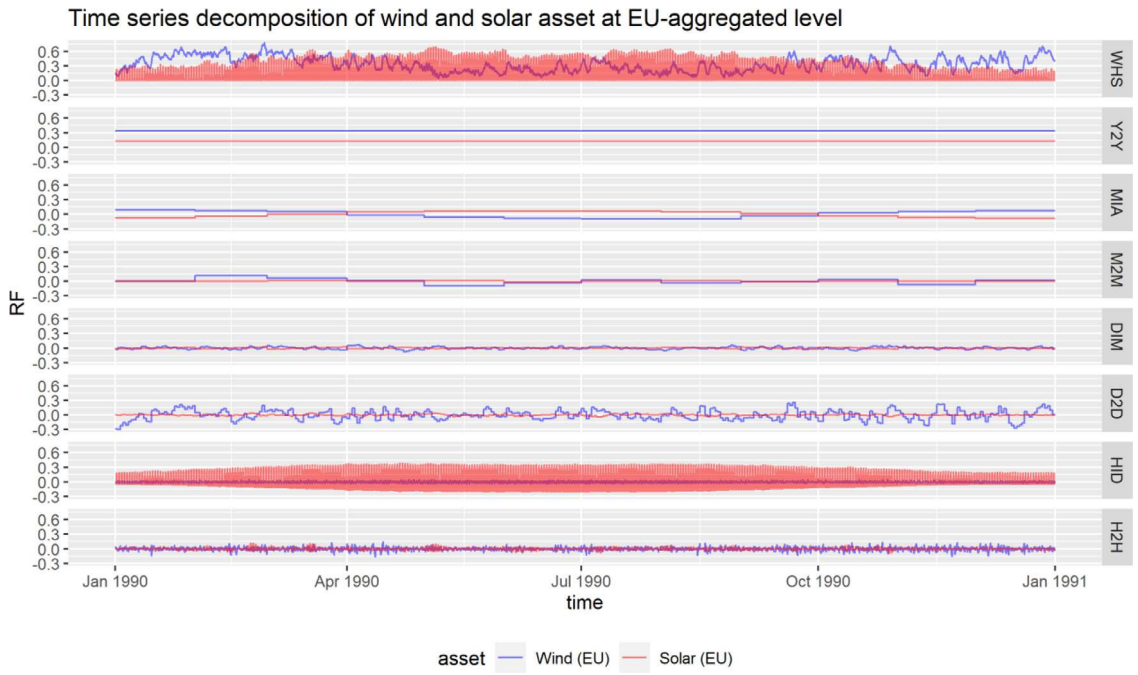


**Fig. 6.** Time series decomposition of wind and solar assets at the EU level.

upper tail [23]. The lower-tail dependence is of particular relevance to renewable energy droughts, which are concurrent extreme low production events of VRE assets. Although Otero Felipe et al. [83]; Raynaud [86]; Ohlendorf and Schill [81] have characterised country-wide historic extreme low production events of single or multiple VRE technologies on a univariate basis for selected European countries, they might be of limited usage to understand renewable energy droughts in interconnected power systems. This study represents the first attempt to assess the intercountry risk of renewable energy droughts and the impact of climate change on such risk. For simplicity and dimension reduction, we focus on two bivariate cases of concurrent extreme low production events. The first case concerns the *cross-border* lower-tail dependence between each country and its directly interconnected neighbours, and the second case the *EU-wide* low-tail dependence between each country and the rest of Europe. Both cases are investigated for solar alone, wind alone, and the mix of wind and solar.

We resort to the conditional probability of concurrent extreme low production events ($P(X \leq x | Y \leq y)$) to measure the lower-tail dependence, where $X$ and $Y$ denote output variables associated with any two paired VRE assets. For instance, in the cross-border case of concurrent extreme low production events for solar, $X$ represents a country-aggregated solar asset and $Y$ represents the other solar asset aggregated at the level of all neighbouring countries. $x$ and $y$ denote the fixed threshold levels defining extremely low production events. Here we define extreme low production events as VRE outputs below the 0.1 quantile level of the output distribution, similar to Otero Felipe et al. [83]. The calculation of the conditional probability of concurrent extreme low production events is based on the empirical copula function. The copula is a joint distribution function characterizing the dependence between random variables but independently from their corresponding marginal distributions [83]. In the bivariate case, the joint cumulative distribution of random variables ($X$ and $Y$) can be described by a copula function $C()$ that links their marginal cumulative distribution functions ($F_X$ and $F_Y$) together:

$$F_{XY}(x,y) = P(X \leq x,\ Y \leq y) = C\big(F_X(x),\ F_Y(y)\big) \tag{33}$$

The marginal cumulative distribution functions transform the random variables X and Y into uniformly distributed margins on the [0,1] interval, which are denoted as $U{=}F_X(X)$ and $V{=}F_Y(Y)$.

We use historic daily wind generation in Germany and France (which represent $X$ and $Y$) to exemplify this transformation in Fig. 7. 7a) shows the scatter plot and histograms for the original random variables $X$ and $Y$, and 7b) for the transformed cumulative margins $U$ and $V$.

According to Sklar's theorem, the copula function is unique if both U and V are continuous.

This means that formula (33) can be rewritten into

$$F_{XY}(x,y) = C(U(x),\ V(y)) = C(u,\ v) = F\big(F_X^{-1}(u),\ F_Y^{-1}(v)\big) \tag{34}$$

Following Bayes's theorem, the conditional probability of concurrent extreme low production events below fixed threshold margins can be calculated based on the copula function:

$$\mathrm{P}(U \leq u | V \leq v) = \frac{\mathrm{P}(U \leq u,\ V \leq v)}{\mathrm{P}(V \leq v)} = \frac{C(u,\ v)}{\mathrm{P}(V \leq v)} \tag{35}$$

Recall that we defined extreme low production events using the 0.1 quantile level as threshold conditions. Consequently, $u = v = P(V \leq v){=}0.1$. Using the empirical copula function, it is possible to estimate the empirical conditional probability of concurrent extreme value events between two VRE assets. To avoid non-continuousness in the marginal distribution of hourly solar RF series due to a large portion of zeros, we aggregate hourly VRE RF series into daily series.[8]

Based on the estimated conditional probability, we also calculate the expected annual number of critical hours (*NoC*) of concurrent extreme low production events in each country for the cross-border and EU-wide bivariate cases:

$$NoC = 0.1 \cdot 8760 \cdot \mathrm{P}(U \leq 0.1 | V \leq 0.1) \tag{36}$$

[8] A large portion of zeros in daily solar production series still exist for Norway and Finland, because the two countries include relatively large areas with solar potentials close to the Arctic Circle with polar nights. This violates the assumption to build up a copula model, which gives NA results. To solve this issue, for these two countries only we exclude winter months (from October to March) of the daily series to estimate the cross-border and EU-wide cases of conditional probability of concurrent extreme low solar production events. This might underestimate the conditional probability, because solar drought events in both countries are expected to be more frequently in winter months. While for other countries, the conditional probability is estimated for the daily series including both winter and summer.

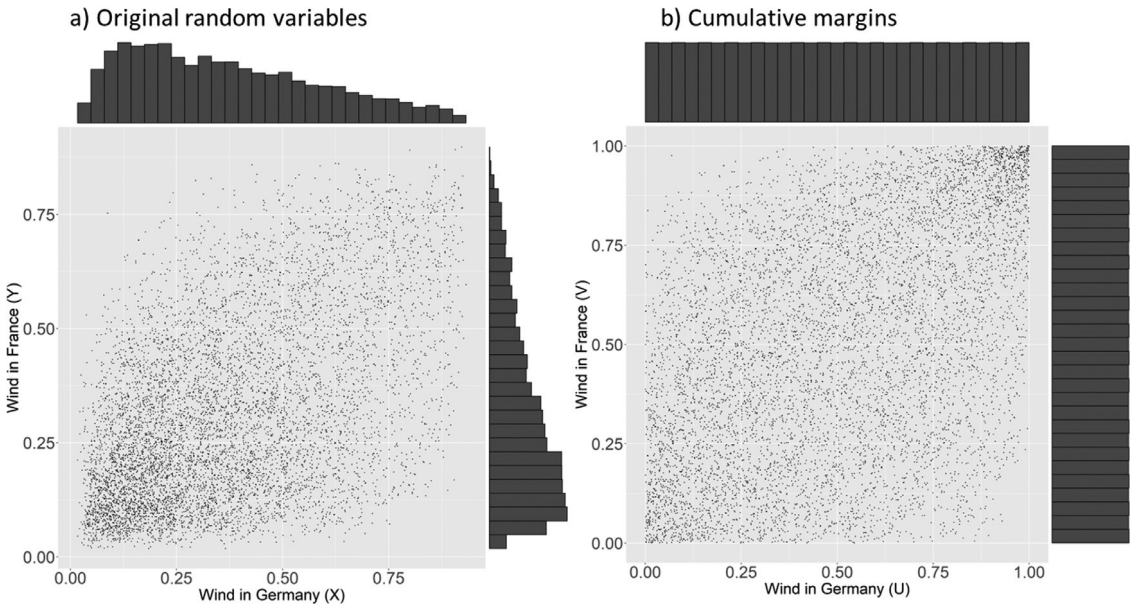


**Fig. 7.** Transformation of random variables into uniformly distributed cumulative margins.

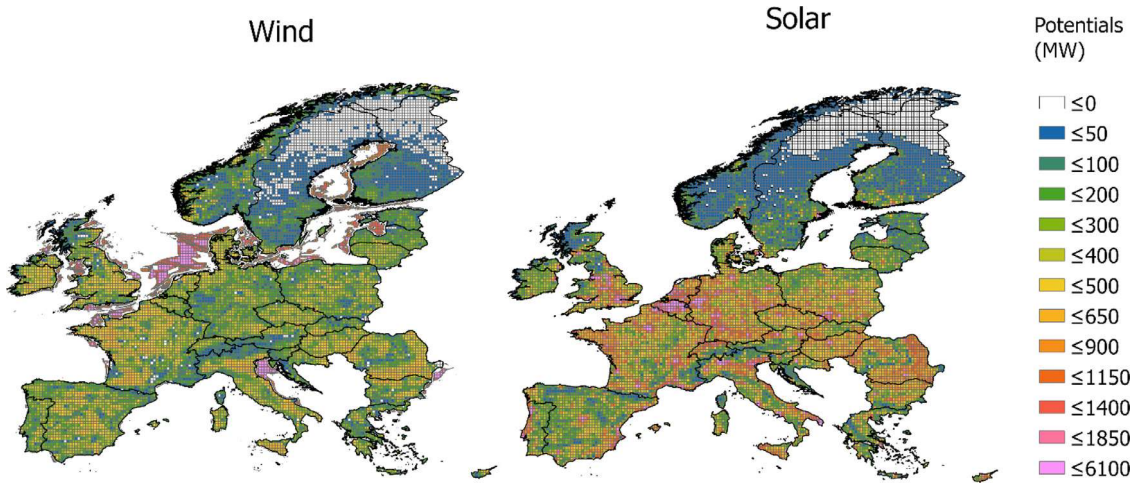


**Fig. 8.** Spatial distribution of geographic potentials of VRE assets across Europe.

## 3. Results

### 3.1. Geographic potentials

The geographic potentials for grid cell based VRE assets across Europe are shown in Fig. 8. Geographic potentials reflect the quantity aspect of VRE resources in terms of maximum installable capacity considering geospatial constraints and land use suitability.

For onshore wind, France, Spain, Germany, Italy, Poland, the UK and Romania have the largest potentials in Europe. Together they account for more than half of total onshore wind potential in Europe (2032 GW). The total offshore wind potentials amount to 918 GW. They are mainly concentrated in the North Sea, the Baltic Sea, the Irish Sea, the English Channel and the Adriatic Sea. Despite a large area, the Mediterranean Sea and the Black Sea are barely suitable for (non-floating) offshore wind development due to the threshold depth of 60 m. The distribution of solar potentials is highly correlated to the urban area for rooftop PV installation. Due to abundant suitable areas for utility PV development, France, Germany, Italy, Spain and Poland lead in solar potentials. The combined share in total European solar potentials (3840 GW) is above 50%.

Owing to policy support and cost reduction driven by technological learning and economies of scale, the deployment of VRE capacity has increased significantly in Europe over the past two decades. At an aggregated Europe level, as of 2021 the currently installed capacities of onshore wind, offshore wind and solar are 192 GW, 28 GW and 175 GW [58], accounting for 9.5%, 3.1% and 4.5% of total potentials of respective technology. For comparison, we present installed capacity and untapped potentials per technology at the country level in Fig. 9. For most countries, there remain large potentials for VRE development. The highest exploitation rates of onshore wind are found in Sweden (25.2%), Netherlands (20.8%), and Luxemburg (20.8%); Netherlands (19%) and Malta (13.6%) of solar. As the frontrunner for investment in onshore wind and solar, Germany has only exploited 33.7% and 11.3% of its potentials, respectively. The exploitation rates of offshore wind at the country level are relatively small. They hardly exceed 3% except for Belgium (68.2%), Germany (11.3%), UK (8.3%). The UK leads offshore wind development in Europe, but more than 91% of its potential are yet untapped. By contrast, due to small total potentials (3.3 GW), the remaining potential for Belgium is only 1.1 GW for developing new offshore wind capacity.

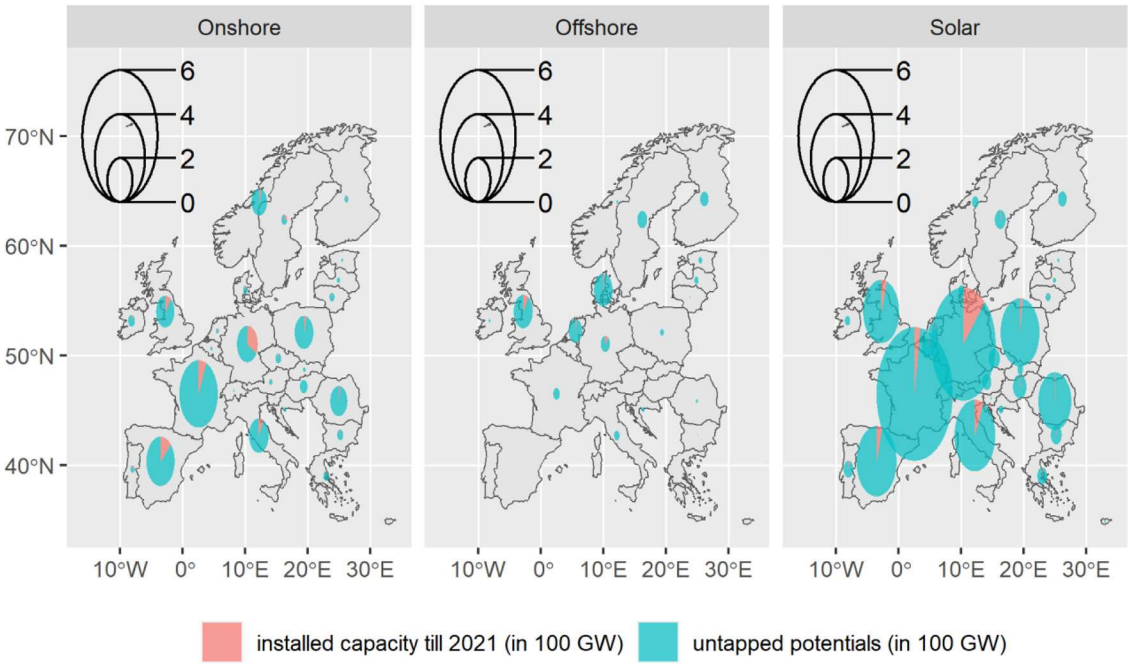


**Fig. 9.** Country-level installed capacity as of 2021 and untapped potentials per VRE technology
Source: based on authors' analysis and IRENA (2022).

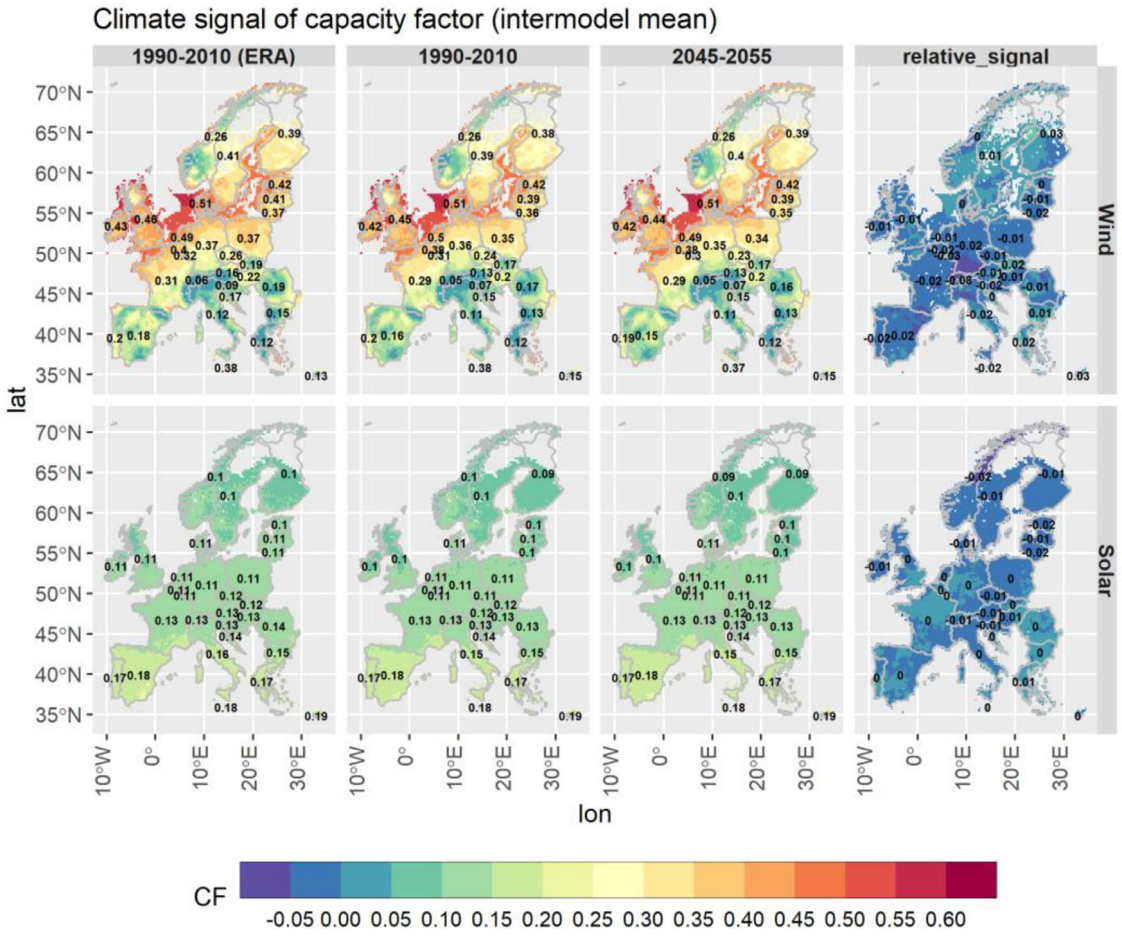


**Fig. 10.** Historic, future and relative climate signal of CF for VRE assets across Europe.

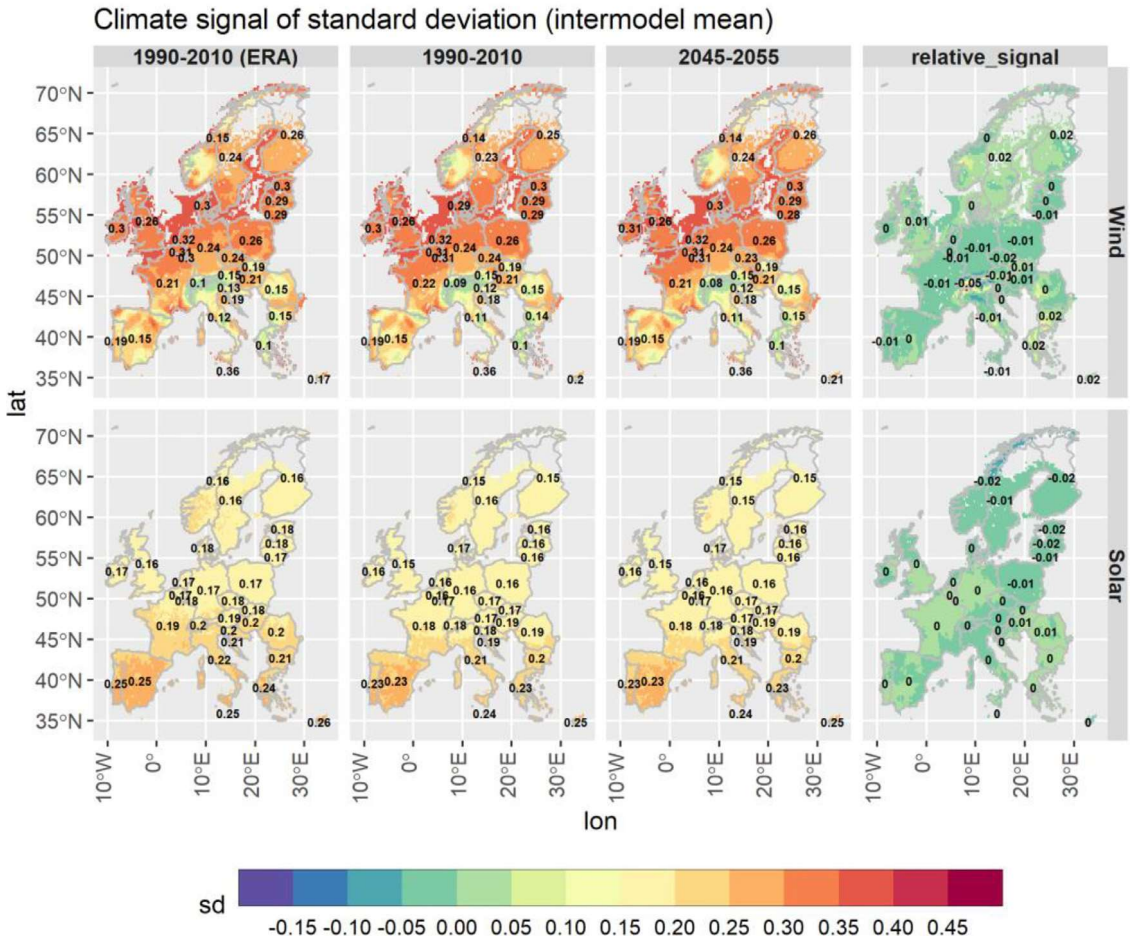


**Fig. 11.** Historic, future and climate signal of raw standard deviation for VRE assets across Europe.

### 3.2. Capacity factor

The historic (1990–2010), future (2045–2055) and relative climate signal (in terms of relative change expressed in decimal fraction) of CF for wind and solar assets across Europe are presented in Fig. 10. The labels represent corresponding country-level aggregated data. For comparison purposes, the historic CF based on ERA data is also shown. The historic CF is in close agreement with the ERA-based historic CF at both grid cell level and country level. Three noticeable results are identified. First, the maximum difference between the two is less than 2 p.p. and 1 p.p. respectively for wind and solar assets. This suggests that climate models can replicate CF well under historic climate conditions. Second, The CF as average normalized outputs per unit of installed capacity reflects the quality aspect of VRE resources. It is shown that the best-quality wind resources in Europe are located in the North sea, the Baltic sea, the Irish Sea, the English Channel and surrounding coastal areas. This can be ascribed to the large pressure difference between the semipermanent Azores High and Icelandic Low, which moves the weather fronts eastward across the ocean [75]. The worst-quality wind resources are located along the major mountains, because of the wind channelling effect in deep valleys [75]. At the country level, Denmark, the Netherlands and the UK have the highest average capacity factor ($\geq$0.45). By contrast, the average quality ($\leq$0.18) of wind resources in Italy and Spain is relatively poor, despite large potentials. As for solar, the CF depends on the local latitude which reflects the difference in solar altitude angle. The highest and lowest CF are respectively found in the South European countries and Nordic countries. Thirdly, the climate signal in terms of the relative difference in CF between historic and future periods seems overall small in magnitude, especially at aggregated country level. The CF of wind decreases in the major part of Europe, except for the Nordic region, the Balkan region and Central Italy. The magnitude of the country-level CF climate signal is hardly above 0.03, except for a large reduction at 0.08 in Switzerland. The country-level CF climate signal for solar is smaller than that for wind. A slight decrease ($\leq$0.02) in solar CF can be observed in Northern and Central Europe. This suggests the impact of climate change under RCP 2.6 on average solar outputs is rather limited.

### 3.3. Raw standard deviation

Fig. 11 shows the spatial distribution of the historic, future and relative climate signal of hourly raw sd for wind and solar assets. The consistency between the climate model-based and the ERA-based raw sd for the same historic period again suggests a fair performance of the climate models in capturing the volatility of VRE supply. The climate signal at the country level is generally small in magnitude for both wind and solar. It hardly exceeds 0.02, with Switzerland (0.05) being the exception.

The spatial distribution of the raw sd follows a comparable pattern to that of the CF, indicating a positive level of correlation. This can be illustrated by the scatter plot of raw sd versus CF for VRE assets at the grid cell level (see Fig. 12). The raw sd and CF respectively measure the (volatility) risk and (expected) hourly return of VRE assets from the perspective of power system operation. Similar to that for financial assets, a tradeoff exists between risk and return. The higher the capacity factor, the higher volatility in the VRE generation profile and hence the greater challenges for grid balancing. Unlike onshore wind assets spreading the

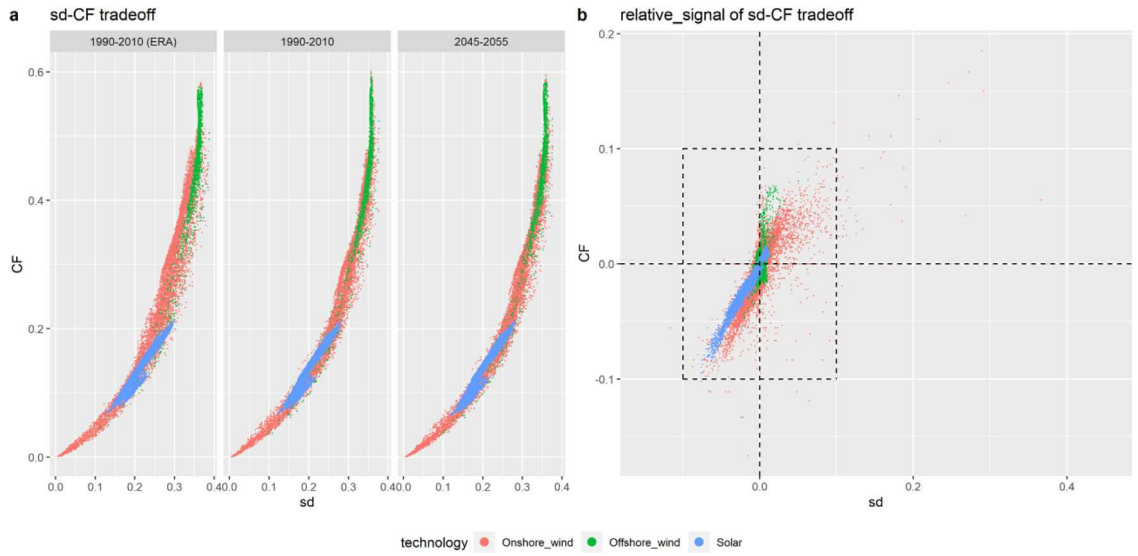


**Fig. 12.** Historic, future and climate signal of risk-return (sd-CF) tradeoff.

entire range of the risk-return profile, the majority of offshore wind assets can be characterised as high-risk and high-return. By contrast, solar belongs to the low-risk and low-return asset group due to the diurnal production pattern. Compared with ERA-based sd, the spread of climate model-based historic sd is relatively narrow across VRE assets at the same level of CF. The same risk-return tradeoff remains for the scatter plot of relative signals with most assets positioned at the first and third quadrants. Except for a limited number of outliers, the signals for both CF and sd are bounded by $\pm 0.1$.

### 3.4. Normalized standard deviation at multiple timescales

Fig. 13 demonstrates the country-level normalized sd of the original whole hourly time series (WHS) and its component time series at different timescales for wind. The normalized sd measures the relative volatility with respect to the mean. Regardless of the timescale, it can be unanimously found that the WHS variability of wind is mainly driven by the variability of the noise terms at D2D and H2H timescales. This means that integration challenge for wind is mainly related to short-term flexibilities, ramping capabilities, and daily & sub-daily energy storage requirements of the power system. Across all timescales, the discrepancy in normalized sd seems to be small between ERA and climate models for the historic period. The climate signal is also small, which is capped by $\pm 0.1$. Notably, the normalized sd decreases over the D2D and H2H timescales close-to-uniformly across Europe, but increases over the DIM and HID timescales. Less seasonal variation in wind output can be expected for the Nordic countries exclusively. This is demonstrated by the decreased normalized sd over the MIA time scale.

In the case of solar, the HID and MIA cycles dominate the WHS variability (see Fig. 14). These two timescales are of respective relevance to the sub-daily system flexibility and seasonal energy storage requirements. Despite a small magnitude ($\leq 0.1$), solar variability decreases in most European countries at all timescales with DIM and MIA being the exception. The increased seasonal solar variation at the MIA time scale occurs mainly in the Nordic countries, France, Germany, Spain and Romania. This suggests the increased need for seasonal storage in these countries.

### 3.5. Correlation at multiple timescales

#### 3.5.1. Country-wide wind-solar correlation

The country-wide wind and solar correlation at different timescales are presented in Fig. 15. Based on historic correlation (calculated from ERA data alone), a negative correlation (anticorrelation) between country-wide wind and solar outputs prevails over Europe. The strength of the anticorrelation depends on the decomposed timescale and the specific country. Noticeably, a very strong anticorrelation ($\leq -0.6$) exists between the seasonal cycles of wind and solar at the MIA timescale, suggesting a large potential for technological complementarity that can be exploited to reduce seasonal variation of VRE outputs. This is particularly useful for countries that lack seasonal energy storage options (e.g., reservoir storage hydropower plants). The strong MIA anticorrelation can be explained by the windy winters of short daytime alternating with the calm summers of longer daytime [75]. Consequently, in a relative sense, it is less pronounced for those countries located in South Europe. This seasonal complementarity is further reinforced by the anticorrelation at the M2M timescale. At other timescales, we also found an overall negative but weaker wind-solar correlation. This indicates daily and hourly It is also consistent with earlier studies, e.g., Schindler et al. [91]; Miglietta et al. [75]; Jerez et al. [60]. Interestingly, at the HID timescale both moderate positive and negative correlations are observed. This implies the presence of regional-specific diurnal wind patterns. The positive correlation mainly exists in countries with large mountain areas and extensive coastlines, due to e.g. foehn and sea breeze [75].

Except for the HID timescale, the climate models show overall good agreement with the ERA data in the determined historic country-wide wind-solar correlation. The correlation is moderately or strongly positive in the climate model-based case at the HID timescale. This indicates the remaining bias of the climate model and its unstastifying performance in capturing the sub-daily comovement between climate variables. Recalling that the original temporal resolution of the climate model is 3 hourly. The pre-processing that linearly interpolates the data to hourly might also contribute to the bias.

The climate signal of country-wide wind-solar correlation is relatively small in magnitude ($\leq 0.2$) across all timescales except for Y2Y, and the sign of correlation hardly changes. This suggests a rather limited mid-term impact of RCP 2.6 on the country-wide wind-solar correlation. At the Y2Y timescale, the largest climate signal ($\sim 0.4$) is found in the UK with the sign of correlation inverting from negative to positive. This implies a non-negligible challenge for the long-term system planning to manage the interannual variability in VRE supply.

#### 3.5.2. Cross-regional wind-solar correlation

The cross-regional correlation matrix enables the investigation of wind-solar technological complementarity beyond the country border. Fig. 16 presents the cross-regional correlation at the WHS timescale as

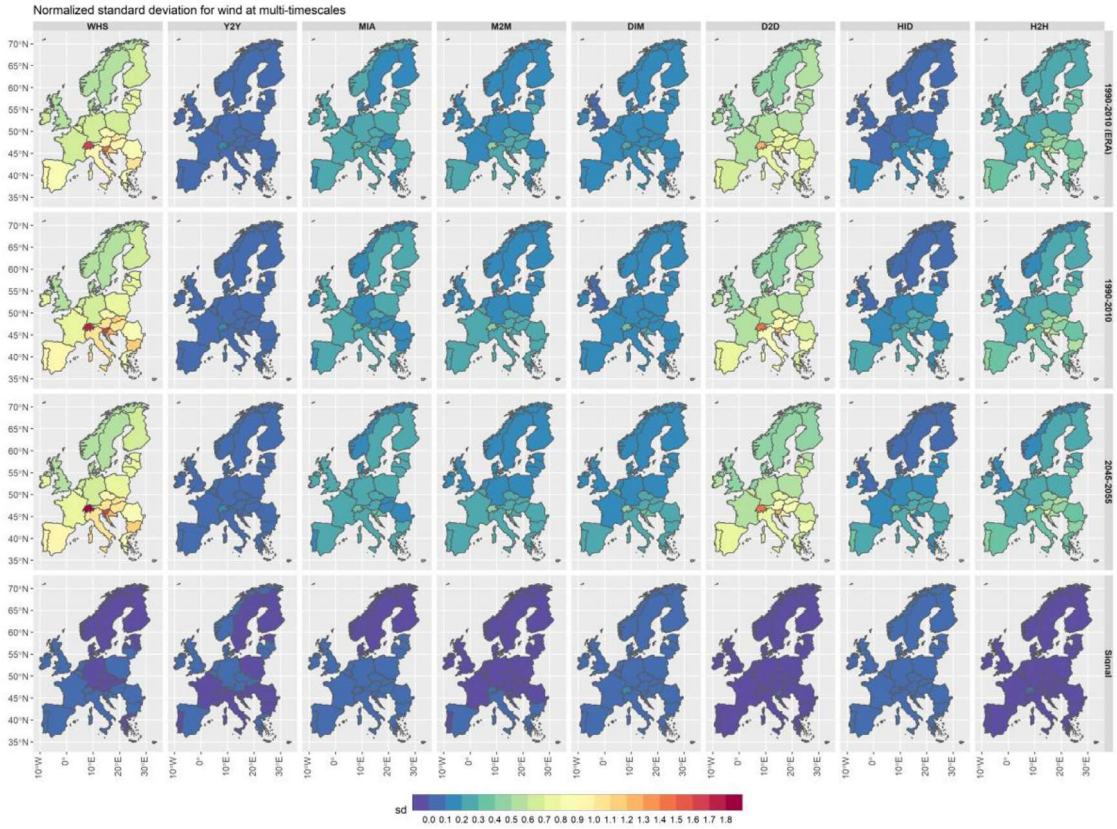


**Fig. 13.** Climate signal of normalized standard deviation for wind across Europe at multiple timescales.

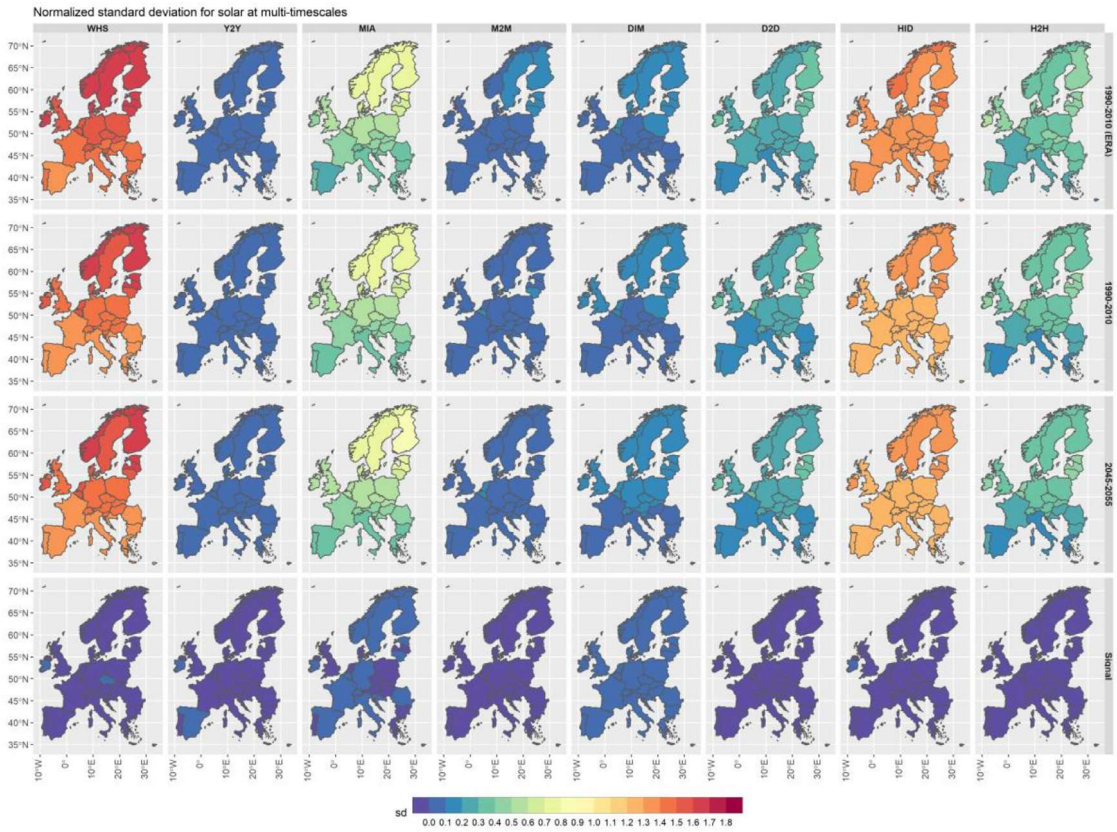


**Fig. 14.** Historic, future and climate signal of normalized standard deviation for solar across Europe at multiple timescales.

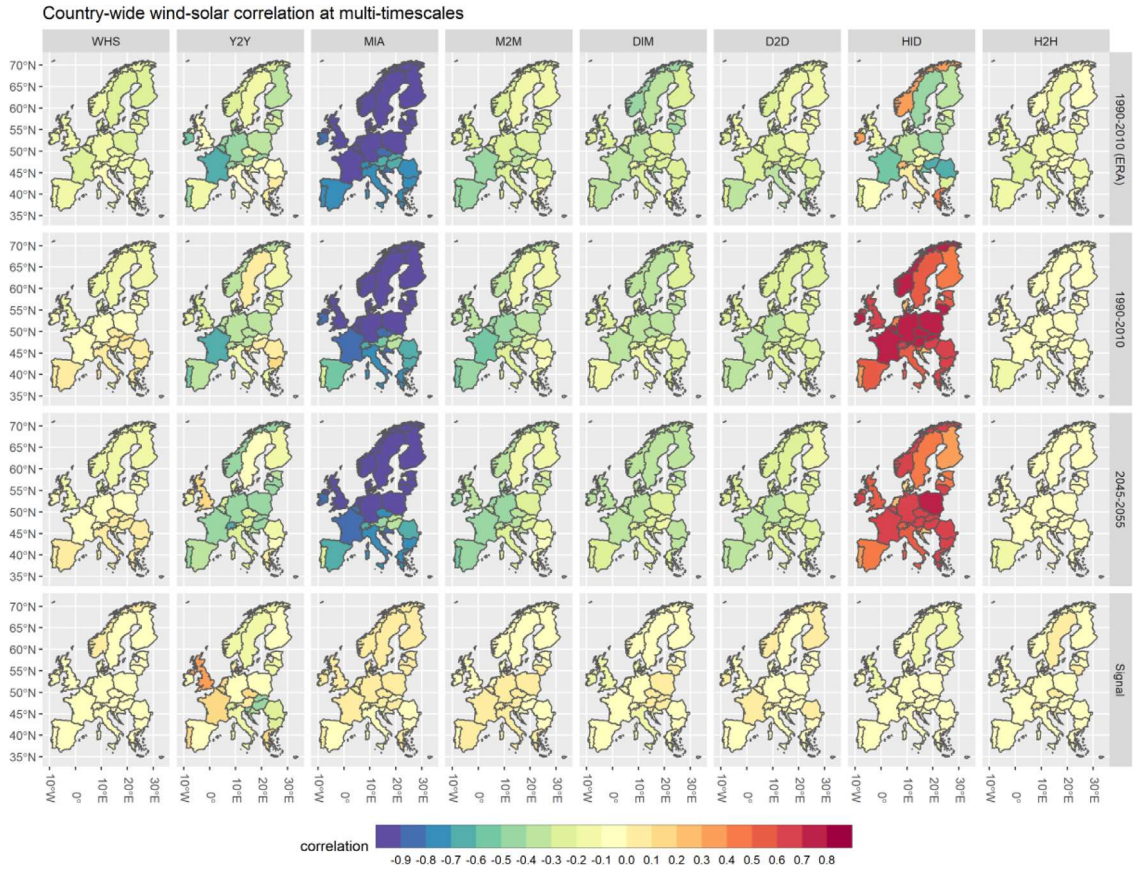


**Fig. 15.** Historic, future and climate signal of country-wide wind-solar correlation.

well as timescales corresponding to the cycle components of VRE generation profiles. The x-axis and y-axis respectively represent wind and solar at an aggregated regional level. Similar to the country-wide correlation, the cross-regional correlation between the cycle components of wind and solar outputs is overall negative based on ERA data. The most pronounced anticorrelation is found at the MIA timescale. In particular, wind in the Baltic, Isles, Nordic, and West regions strongly complements solar in all regions (with an anticorrelation above 0.9). The large potential of seasonal technological complementarity can save demand for seasonal storage. This brings about co-benefits for the EU's ongoing efforts in establishing a European internal electricity market [31], which requires large-scale investments in the pan-European transmission network. We also observe moderate wind-solar anticorrelation is also observed at the HID timescale between certain regions, notably between wind in France and solar in other European regions, and between wind in Iberia and solar in the East, Baltic and Balkan. This suggests diurnal technological complementarity. Except for the HID timescale, the climate model-based correlation for the other cycle components tends to be consistent with that based on ERA data. In addition, the climate signal of cross-regional correlation tends to be small, and it hardly exceeds $\pm 0.1$. This suggests limited impacts of climate change under RCP 2.6.

For the noise components, the cross-regional wind-solar correlation is presented in Fig. 17. Although at the Y2Y and M2M timescales, moderate correlations can be observed between certain regions, for the other timescales the wind-solar correlation of the noise components is much weaker. Unlike the cycle components that tend to have a negative cross-regional correlation, at the Y2Y and M2M timescales the sign of correlation for the noise terms is less distinct depending on the paired regions. For instance, a moderate anticorrelation exists between wind in Iberia and solar in France and Alpine at the M2M timescale. This can reinforce the wind-solar seasonal complementarity at the MIA timescale, By contrast, the moderate positive correlation between wind in Nordic and solar in Iberia at the M2M weakens the seasonal complementarity. From a system planning perspective, wind in France seems to be an ideal investment option, as its generation profile tends to be negatively correlated with solar in other European regions at almost all timescales. Once again, consistency is observed between the cross-regional correlation based on the climate model and that is based on ERA data. The climate signal of the cross-regional correlation seems negligible for the noise components at the M2M, D2D and H2H timescales. As for the Y2Y timescale, some moderate climate signals can be observed for a few paired regions, e.g., between wind and solar in France and Iberia.

### 3.6. Conditional probability of concurrent extreme low production events

#### 3.6.1. Cross-border concurrent renewable energy drought events

Fig. 18 presents the historic, future and climate signal of the conditional probability of cross-border concurrent renewable energy drought events across Europe for wind, solar and the mix of wind and solar. The cross-border conditional probability indicates the likelihood of renewable energy droughts in each country given the occurrence of renewable energy droughts in neighbouring countries. The labels indicate the expected annual number of critical hours per country when concurrent renewable energy droughts occur. First, the climate model seems to simulate very well the historic climate based on the ERA data. Secondly, the climate signal of renewable energy drought events under RCP 2.6 seems also marginal, as the conditional probability change never goes beyond $\pm 0.05$. Thirdly, the susceptibility to cross-border renewable energy drought events depends on the country and the VRE technologies. In the case of wind alone, Latvia, Estonia, Bulgaria, Germany, and the Netherlands are most susceptible to renewable energy droughts

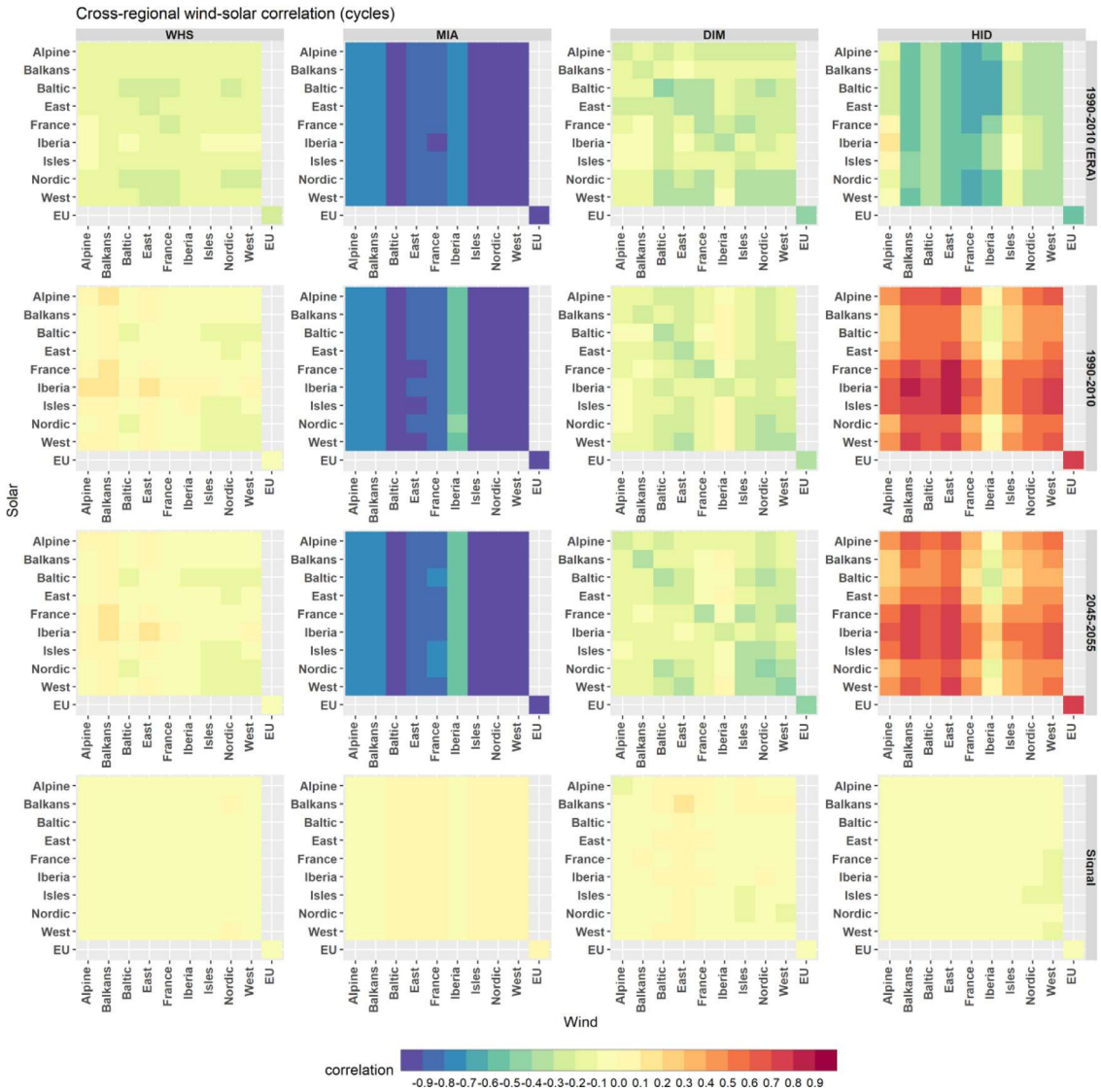


**Fig. 16.** Historic, future and climate signal of cross-regional wind-solar correlation (cycle components).

with a conditional probability above 0.5. The left tail of wind profiles between these countries is apparently highly dependant on those of their interconnected neighbours. The cross-border renewable energy drought risk for solar alone is larger due to high synchronicity in solar profiles between neighbouring countries. The mix of wind and solar seems to moderately reduce the cross-border conditional probability of renewable energy drought events compared to solar alone, suggesting a benefit of technological diversification. However, compared to wind alone, the benefits of a mix are more observable in the countries in the north half of Europe where wind potentials dominate the share of the technology mix. For the mixed case, cross-border renewable energy drought events occur most frequently in countries located in the Baltic region and Southeast Europe. Hence, these countries may need more backup capacity to manage the tail risk associated with renewable energy droughts if power exchange is only allowed with direct neighbours.

### 3.6.2. *EU-wide renewable energy drought events*

The analysis of the EU-wide renewable energy drought events (see Fig. 19) is based on the copperplate assumption that all European countries are perfectly interconnected. The EU-wide conditional probability indicates the likelihood of renewable energy droughts in each country given the occurrence of renewable energy droughts in the rest of Europe. The labels indicate the expected annual number of critical hours of concurrent EU-wide renewable energy droughts. Similar to the cross-border case, the EU-wide conditional probability per country based on the climate data is close to that based on the ERA data. The climate signal of the EU-wide conditional probability is negligible. Compared with the cross-border case, the EU-wide conditional probability of renewable energy drought events for most countries is reduced for wind, solar and the mix of wind and solar. This means that geographic diversification is helpful to reduce tail risk of concurrent renewable energy droughts. However, even under the copperplate assumption, the EU-wide conditional probability remains pronounced and non-negligible. As in the case of mixed wind and solar, it ranges from 0.20 to 0.56, depending on individual countries. Therefore, the EU-wide conditional probability of concurrent renewable energy droughts can be interpreted as a non-diversifiable systemic risk. To address this systemic risk, sufficient flexibility resources other than interconnectors are required. Moreover, we also find that for a limited number of countries the EU-wide conditional probability is slightly higher than the cross-border case. An example is solar energy droughts in France. This is because the left tail distribution of solar in France is more synchronous to that at the aggregated EU level. A similar situation is observed for Poland in the mixed

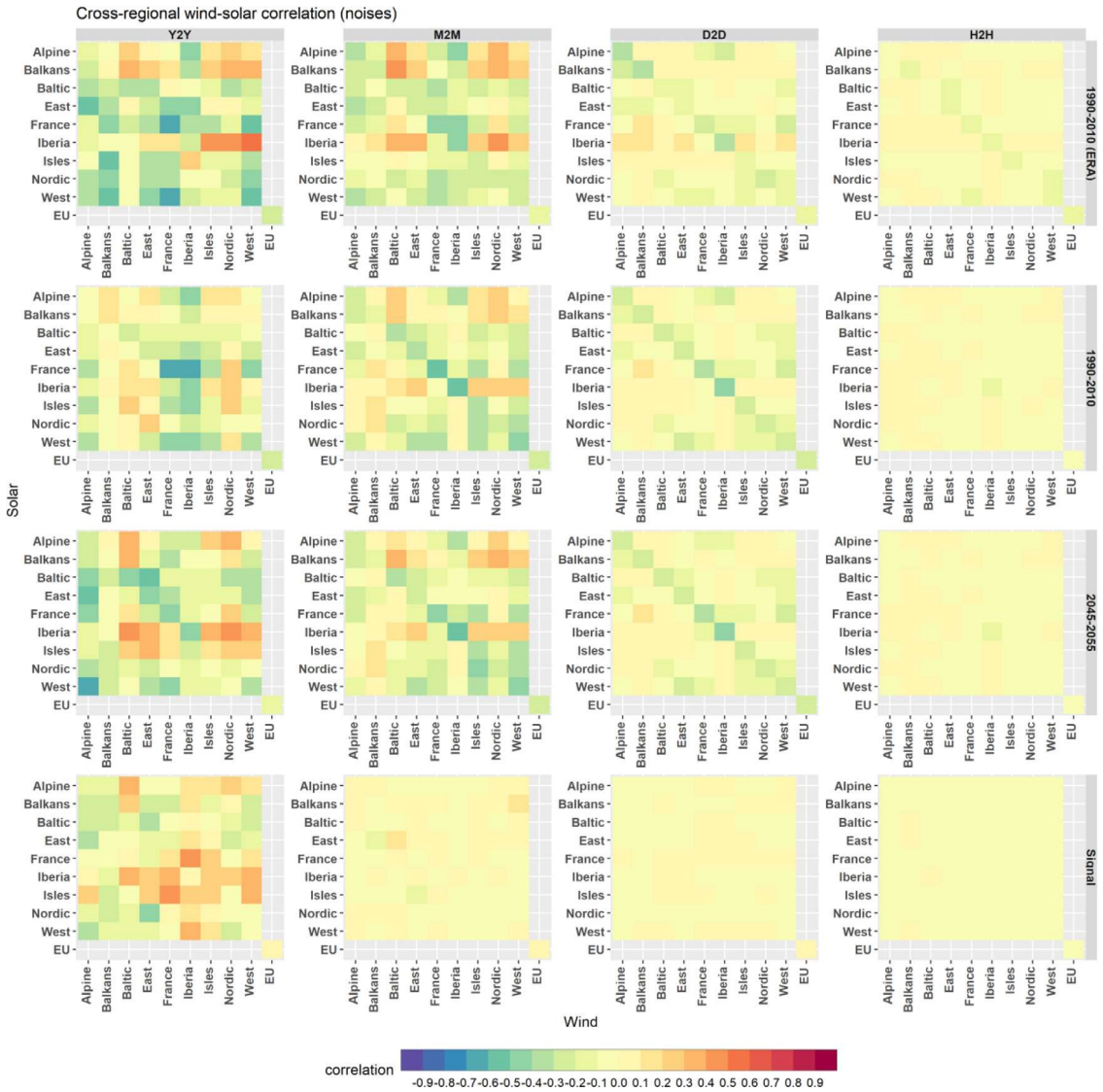


**Fig. 17.** Historic, future and climate signal of cross-regional wind-solar correlation (noise components).

case, despite a small difference between the cross-border and EU-wide conditional probabilities.

## 4. Discussion

### *4.1. Limitations and caveats*

Due to data and scope, a few limitations can be identified in this study. Here we discuss the most prominent limitations and potential caveats for the interpretation of the results.

#### *4.1.1. Data consistency*

This study relies on a large number of data from multiple sources. They can be grouped into two main streams: climate data and meteorological reanalysis data to characterise generation profiles of VRE supply and associated statistical measures; geospatial data for determining geographic potentials for VRE installation. The use of data based on multiple sources can give rise to data consistency issues.

- Geospatial data

Data consistency is less likely to be a concern for the used geospatial data, because they mainly include topographic and bathymetric information and land cover data that are unrelated to each other. The mismatch between geographic boundaries of polygon-based shapefiles (e.g., maps of terrestrial territory and exclusive economic zone) and grid-cell based raster data (e.g., elevation and land cover data) can introduce potential error propagation in geospatial analysis, but the impact is expected to be marginal due to high-resolution of the data.

- Climate data

Another source of data inconsistency results from the inherent limitations of climate data simulated from the combination of GCM and RCM. First, climate data consisting of standard variables is only bias-adjusted on the daily scale while uncorrected sub-daily anomalies are superimposed. The bias-adjustment procedure uses meteorological reanalysis data as the reference, which increases consistency between the two datasets. Since we have identified an overall agreement between key statistical measures of VRE profiles based on climate data and reanalysis data for the same historic period, the remaining unadjusted biases are relatively small. However, the limitations of the bias adjustment at a sub-daily time scale become apparent when analysing the cross-regional wind-solar correlation characterised at a sub-daily hourly timescale (see section 3.5). A moderate or positive strong correlation is found in the climate data-based case, while a negative cor-

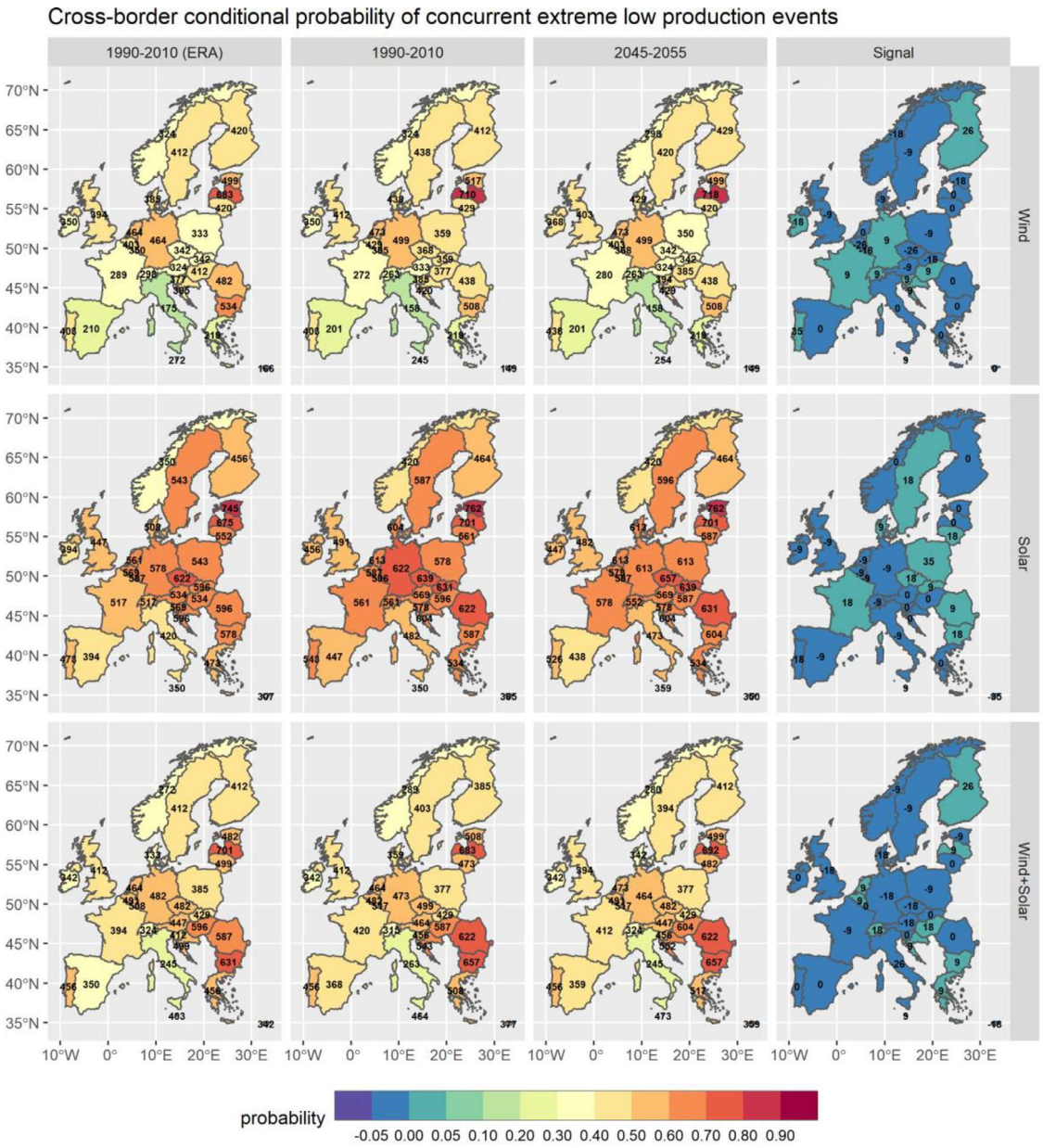


**Fig. 18.** Historic, future and climate signal of conditional probability for cross-border energy drought events.

relation is predominantly observed based on the more accurate reanalysis data. This suggests an unsatisfied performance of the climate model in capturing the sub-daily comovement between climate variables. Secondly, to obtain hourly VRE time series, the climate data fed into the energy conversion model is linearly interpolated from the original 3-hourly resolution to 1-hourly resolution. This might also induce bias with regard to statistical measures that are evaluated at sub-daily timescales. Finally, unlike reanalysis data, climate data only offers limited standard variables that can be directly used for energy conversion. For instance, the only variable relevant to wind energy conversion is surface wind speed at 10 m. Consequently, assumptions with regard to surface roughness or shear exponent must be made to extrapolate wind speed to turbine hub height. This can lead to a potentially large error propagation due to the cubic relation between wind speed and wind power. This study derives site-specific shear exponents based on a regression between two wind speeds at 10 m and 100 m of (historic) reanalysis data. Despite being more accurate than other simplistic assumptions, the approach presumes the same static shear exponents to be persistent over the future. Overcoming these limitations of climate data calls for the development of better bias-adjustment methods, increased temporal resolution of climate modelling, and the expansion of standard climate variables within the climate modelling community.

#### 4.1.2. *Limited ensemble size and intermodel uncertainty*

Ideally, a large set of climate models would be used to simulate climate projections to capture the intermodel uncertainty of climate signals. Due to the computation costs of both RCMs (for downscaling) and the energy conversion model, the ensemble size of climate projections and the selected length of time periods (10–20 years) were therefore limited for the impact assessment. While the climate projections driven by 3 different GCMs were selected to cover the spread of climate signals within the given RCP 2.6 as good as possible, the limited ensemble size may contribute to uncertainties in the results. As the aim of this study is to provide a best estimate of climate signals in terms of the intermodel ensemble mean rather than quantifying the intermodel uncertainty, the

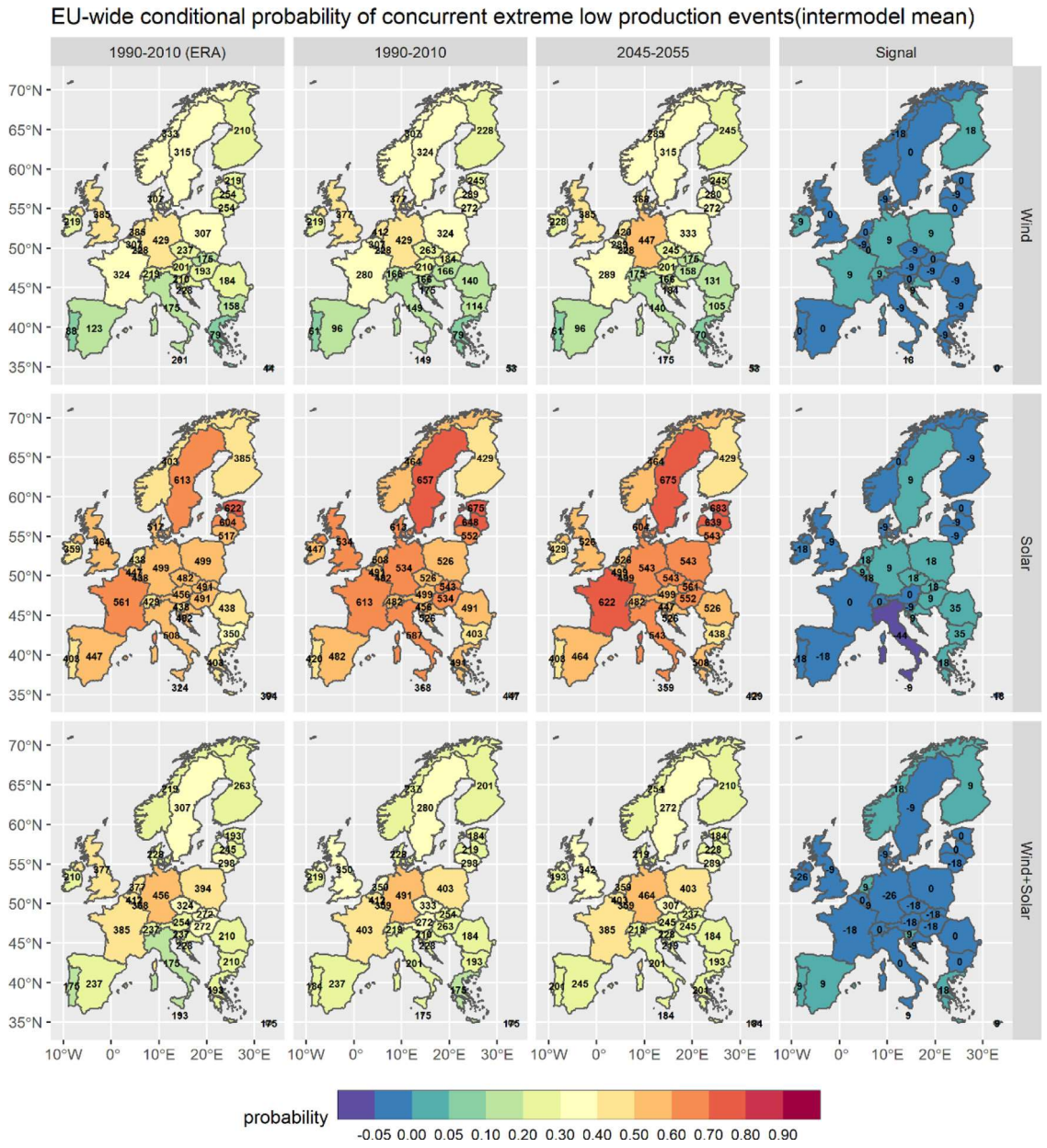


**Fig. 19.** Historic, future and climate signal of conditional probability for EU-wide renewable energy drought events.

limited ensemble size can be reasonably justified. Another uncertainty source comes from the relatively shorter selected length of time periods, which may open up a potential influence of the internal variability of the determined climate signals.

#### 4.1.3. *Conversion efficiency degradation and improvement*

One merit of the present study lies in the comprehensive energy conversion model developed for impact assessment, which enables a more realistic determination of VRE generation profiles compared to other studies. For instance, the wind energy conversion factors into location-specific power law profiles of wind speed, elevation-adjusted single turbine power curves, multi-turbine power curves representing spatial propagation of wind speed, and wind speed-dependant wake losses. As for solar PV, both location-specific empirical panel angles and efficiency losses due to non-standard operating conditions are considered. Despite a large number of input parameters, the application of the detailed energy conversion model can be repeated for other regions of the world. This is because all inputs are based on the standard variables of climate data, open access meteorological reanalysis data and geospatial data, and reasonable assumptions consistent with the literature. However, the model does not capture every factor affecting energy conversion. A limitation of the model is that we assume a constant performance of VRE technologies under standard test conditions over the entire lifetime. On the one hand, the efficiencies of both wind turbines and solar PV deteriorate with age, with an average annual degradation rate of 1.6% per year [94] and 0.8% per year [62] respectively. Hence, VRE generation determined in this study may be overestimated. On the other hand, the energy conversion model is built upon representative commercial modules of present-day VRE installations. Assuming potential efficiency increases with technological improvement, we may underestimate future VRE generation. Exploring the joint impacts of ageing-related degradation and technological improvement on VRE generation is important to understand the lifecycle economics of VRE technology, which can be recommended for future research. However, they are unlikely to affect the main results of this research with regard to the impact of climate change on VRE generation.

#### 4.1.4. Lack of future land cover data

Geographic potentials of VRE assets depend on suitable areas per land cover class. This study does not consider land cover change and its impact on future geographic potentials. The same geographic potentials based on the historic land cover map are assumed to be constant over time. Both climate and socioeconomic changes can affect land use patterns and land cover [26]. Integrated impact assessment models have already been used to project future land cover development, despite a relatively low resolution and limited land cover classes. Further research is recommended to explore the evoluation of geographic potentials in relation to land cover change over time.

#### 4.1.5. Methods for geographic aggregation

Depending on different analysis purposes in this study, VRE profiles are aggregated from grid cell level to country or regional level for a single VRE technology or a mix of VRE technologies. Geographic potentials of VRE assets per grid cell are used as weights to characterise a representative "average" generation profile within a geographic boundary. This implies the deployment and allocation of VRE capacity are assumed to be proportional to the maximum installable capacity per VRE asset across space and technology. This approach is justifiable in absence of pre-specified information regarding future installed capacity per VRE asset. However, as long as the total potentials are not fully tapped, other capacity allocation options are plausible. For instance, investors can prioritize VRE investments at sites with the highest net profits or capacity factors. System operators may prefer the deployment of VRE capacity close to the demand centre. There also exist policy scenarios prescribing the optimal share of each VRE technology in the future capacity mix per European country. Future studies can be carried out to investigate the impact of alternative capacity allocation methods on the aggregated generation profile.

#### 4.1.6. Size of VRE technologies, demand profile and storage

One delineation of this study is that the size (installed capacity) of VRE technology in the mid-term future European power system is not determined, since we only characterize VRE supply on the basis of per unit of installed capacity. Being not the core focus of climate impact studies concerning VRE supply, the size of installed VRE capacity is often either disregarded [15,21,24,39,52,53,110], assumed at frozen historical level [98,100], or prescribed at a fixed level from other scenario studies [5,60]. Determining the cost-optimal size of VRE capacity is important for planning and operation of the power system, but it also depends on many other factors not considered in this study.

As the power system must ensure grid balancing between supply and demand, both the volume and pattern of electricity demand may strongly affect the technology mix of electricity supply [65]. In particular, due to limited load-following capability, the size and uptake of VRE can be constrained by the demand pattern. Bossmann (2013) found that electricity demand with higher diurnal variations mainly increases the need for dispatchable generation capacity instead of VRE capacity to meet peak demand. The reliable projection of long time series of future demand profiles is of high relevance but a challenging research area, because multiple factors affect the evolution of both the magnitude and pattern of electricity demand over time. They include socioeconomic development (e.g. population, urbanization, gross domestic product), energy efficiency improvements, behavioural change for electricity saving, electrification trend of end-use sectors (e.g. transport with electric vehicles, space heating & cooling with heat pump and air conditioning) and development of electrofuels [66,76]. Electrification further increases the dependency of electricity demand on the variability and change of climate conditions, because both heating and cooling demand is a function of ambient temperature and solar irradiance. The rising average temperature also leads to less heating in winter, but more cooling in summer [89]. Meanwhile, given the increasing penetration of smart metering and real-time pricing, electricity demand is also expected to be more flexible and price-responding [27,54]. Numerous studies have projected future electricity demand at various geographic scales, but none have considered these factors in a comprehensive manner. Many of them simply scale historic demand patterns to a projected or extrapolated future demand level, disregarding changes in demand patterns [6]. Zappa and van den Broek [111], Bobmann and Staffell [6], Bossmann et al. [10], and Staffell & Pfenninger [96] have explored the structural change of demand patterns in relation to electrification and/or energy efficiency measures, but they do not consider climate change. Castillo et al. [16], Isaac and van Vuuren [59], Zhang et al. [112], and Fan et al. [37] have included the average impact of climate change to project electricity demand, despite a low spatiotemporal resolution which is insufficient to generate chronological hourly demand profile. We suggest scenario-based sector-specific bottom-up studies to further investigate this area and associated uncertainties. For instance, the framework combining shared socioeconomic pathways (SSPs) and representative concentration pathways (RCPs) used by the integrated assessment models (IAMs) community [105] seems promising to explore the scenario space of plausible demand profile projections.

The size and uptake of VRE capacity can also be increased by complementary storage technologies, such as pumped storage hydropower, battery and hydrogen storage [41]. This is because energy storage smooths out the fluctuations of VRE outputs and improves the load-following capability of VRE at different timescales. However, determining the cost-optimal full technology mix (including VRE, storage technologies, and dispatchable generation technologies) in a decarbonized future power system and examining its reliability requires detailed modelling of the power system in terms of capacity expansion and economic despatch. It is also dependant on many uncertain factors, such as future demand profile, fuel price, carbon price, and cost development of different power generation and storage technologies. Studies exist using the power system model to explore future technology mix, but they are often based on historical VRE generation profiles [14,65,111], use inconsistent VRE generation and demand profiles corresponding to different weather years [104], or ignore interannual variability [12,49]. This points out new directions for future research. Our analysis provides essential inputs for the power system modelling in terms of VRE profiles characterised under future climate conditions. The strong wind-solar seasonal complementarity at the cross-regional level identified in this study also provides a rationale to develop strategies optimizing the sites of VRE assets, which serves as an alternative non-technological option to seasonal storage technologies (e.g., reservoir storage hydropower plant, hydrogen storage) for managing the seasonal fluctuations of VRE supply. The relative pros and cons in terms of costs and benefits can be investigated through power system modelling in future studies.

### 4.2. Comparison with other studies

Since most climate impact studies focus on the projected change of average VRE production, we only compare the results with other studies in this regard. We find an overall reduction in average wind and solar production for most of Europe between the 1990–2010 period and the 2045–2055 period. The relative change of average VRE production is rather limited in magnitude at the country level, which is within ±3% for wind (except for Switzerland) and ±2% for solar. However, a direct comparison with other studies remains difficult. This is because only a limited number of studies investigate the mid-term impact of climate change on European VRE supply under RCP 2.6 or comparable warming conditions. amongst these studies, our findings corroborate with Kozarcanin et al. [71] and Tobin et al. [98] for both wind and solar in terms of directions and strengths of changes, and Gao [39] for solar. Nevertheless, our results also seem to disagree with others. For instance, Gernaat et al. [40] and Hou et al. [53] estimated an overall increase in solar generation across Europe. Hosking et al. [52] found wind outputs increase for the majority of Europe, with the greatest increase in the UK (up to 10%) but a negligible decrease in the South. The discrepancy between studies might also be explained by different

GCM-RCM combinations for climate simulation and levels of detail of the energy conversion model used. This calls for better harmonization of climate scenario development, energy conversion method and other key assumptions in future studies.

## 5. Conclusion

This paper assessed the geographic potentials for VRE technologies in Europe, considering multiple spatial constraints and land cover classes. The total potentials for onshore wind, offshore wind and solar are 2032 GW, 918 GW and 3840 GW, respectively. Accounting for more than half of the total potentials in Europe, France, Spain, Germany, Italy, Poland, the UK and Romania have the largest potentials for onshore wind development. Offshore wind potentials are mainly concentrated in the North Sea, the Baltic Sea, the Irish Sea, the English Channel and the Adriatic Sea. Despite a large area, the Mediterranean Sea and the Black Sea are barely suitable for (non-floating) offshore wind development due to a sea depth above 60 m. The distribution of solar potentials is highly correlated to the urban area for rooftop PV installation. With abundant suitable areas for utility PV development, France, Germany, Italy, Spain and Poland lead in solar potentials. The already installed capacities of onshore wind, offshore wind and solar as of 2021 in Europe are 192 GW, 28 GW and 175 GW, which account for 9.5%, 3.1% and 4.5% of total potentials of respective technology. Therefore, there remain large untapped potentials for VRE development.

Based on a comprehensive energy conversion model, this study also characterised the historic, future, and projected changes of European VRE supply under RCP2.6 from aspects of average production, production variability, spatiotemporal complementarity, and risk of concurrent renewable energy droughts.

We find an overall reduction in average wind and solar production for most of Europe between the 1990–2010 period and the 2045–2055 period, except that wind increases in Nordic countries and solar increases in Northwest Europe and the Balkans. At the country level, the climate signal of average production is rather limited in magnitude. The relative percentage change for wind is within $\pm 3\%$ (except for Switzerland) and $\pm 2\%$ for solar. Besides average production, the projected mid-term changes in other aspects of VRE supply are also relatively small. In other words, the expected impact of climate change on European VRE supply is less of a concern if we strictly follow a Paris-proof emission reduction pathway. This adds another rationale for policymakers to support early and stringent climate change mitigation efforts.

Based on a spectral analysis, we demonstrate that the variability of hourly wind generation series is mainly driven by the day-to-day and hour-to-hour variations, whilst intraday hourly and intra-annual monthly cycles dominate the variability of hourly solar generation. The same analysis also enables the identification of multi-timescale technological complementarity between wind and solar assets at the cross-regional level. The seasonal cycles of wind and solar exhibit strong complementarity, which hold under both historic and future climate conditions. This is indicated by an anticorrelation ranging between $-0.6$ and $-0.9$, depending on paired regions. Effectively harvesting wind-solar complementarity can mitigate the source variability of VRE outputs at the intra-annual monthly timescale and provides an alternative option to seasonal storage. It requires efforts from policymakers to accelerate the development of pan-European transmission infrastructure and harmonise the coordination of cross-border planning and siting of VRE deployment, which is also consistent with the EU's policy objective to establish the internal electricity market.

Furthermore, the intercountry risk of concurrent daily renewable energy drought events was investigated, which hardly changes between the investigated historic and future periods. In the cross-border case where energy exchange is exclusively between each country and its neighbouring countries, the risk of solar droughts is large over the entire Europe due to high synchronicity in solar profiles. Technological diversification through mixing solar with wind can moderately reduce the renewable energy drought risk. For the wind-solar mix, countries located in the Baltic region and Southeast Europe are most susceptible to cross-border renewable energy droughts with a conditional probability above 0.5. Compared with the cross-border case, the risk of EU-wide concurrent renewable energy droughts for most countries is reduced for wind, solar and the wind-solar mix. This demonstrates the benefits of geographic diversification. However, even under the copperplate assumption, the risk of concurrent renewable energy droughts remains non-negligible (with a conditional probability between 0.20 and 0.56) . In the case of wind-solar mix, Central Western European countries and Poland are most likely to experience concurrent renewable energy droughts given the occurrence of renewable energy droughts in the rest of Europe. The adequacy of flexibility resources in relation to concurrent renewable energy droughts must be considered by system operators when planning future weather-resilient energy systems for these countries.

## Declaration of Competing Interest

The authors declare that they have no known competing financial interests or personal relationships that could have appeared to influence the work reported in this paper.

## Data availability

Data will be made available on request.

## Acknowledgements

This work is part of the research programme "Evaluating sediment Delivery Impacts on Reservoirs in changing climaTe and society across scales and sectors (DIRT-X)" with project number 438.19.902, which is financed by the European Research Area Network (ERA-NET). We acknowledge the World Climate Research Programme's Working Group on Regional Climate, and the Working Group on Coupled Modelling, former coordinating body of CORDEX and responsible panel for CMIP5. We also thank the climate modelling groups (listed in Table 1 of this paper) for producing and making available their model output. We also acknowledge the Earth System Grid Federation infrastructure an international effort led by the U.S. Department of Energy's Program for Climate Model Diagnosis and Intercomparison, the European Network for Earth System Modelling and other partners in the Global Organisation for Earth System Science Portals (GO-ESSP). The authors are also grateful to Laurens Stoop for his support of data provision and inspiring discussions. We also appreciate the anonymous reviewers for their valuable comments.

## Appendix

Table A1 provides a detailed review of state-of-the-art literature covering climate impacts on VRE supply. Most relevant information is summarized for each study, including climate scenario, the usage of regional climate model for downscaling and associated resolution, ensemble size of climate scenario, long-term period studied, technology considered, region, levels of detail of energy conversion model, statistical measures used to characterise VRE supply and main conclusion.

**Table A1**
Summary of existing studies of climate change impacts on future VRE supply.

| Paper | Climate scenario (in terms of RCP) | Whether regional climate model is used (Y/N) for downscaling and associated resolution | Ensemble size per climate scenario | Long-term period studied | Technology (if the wind is not specified as onshore or offshore, it is denoted as wind)or climate variable | Region | Levels of detail of energy conversion model (N.A./Very Simplistic/ Simplistic/Detailed) | Statistical measures | Main conclusion |
|---|---|---|---|---|---|---|---|---|---|
| [67] | RCP 4.5 & 8.5 | Y (5 km; daily) | N.A. | 1980–2004; 2020–2044 | Wind speed | Greece | Very simplistic: Power law with uniform shear exponent 1/7; theoretical power density method | Mean wind speed; Weibull shape parameter; theoretical wind energy density; return period associated with extremely high wind (40 m/s); friction velocity | Projected change in mean annual wind speed varies locally between −5% and +20%; whereas between −15% and +60% for wind energy density; increases in extremely high wind speed |
| [93] | RCP 4.5 & 8.5 | Y (12 km or 9 km depending on RCM used but nested 27 km; daily) | 14 | 1971–2000; 2071–2100 | Offshore wind | Western Iberian | Very simplistic: log law with uniform roughness length for sea ($1.52\times10^{-4}$ m); three-step power density method for wind | Mean wind speed and outputs | Projected reduction in wind speed and wind power for all seasons across a majority of ensemble members, with an exception for summer; signals for RCP 4.5 is less strong than RCP8.5. |
| [110] | RCP 2.6, RCP 4.5 & RCP 8.5 | Y ($12.5\ km^2$; hourly) | 3 for RCP2.6 and 5 each for RCP 4.5 & RCP 8.5 | 2010–2039; 2040–2069; 2070–2099 | Wind and PV | Seven European cities reflecting five climate zones | Very simplistic: power law with uniform exponents for wind; theoretical power density method; PV conversion does not consider the inclination | Mean wind and PV outputs; correlation between outputs and temperature | Long-term mean wind and PV generation do not change considerably (below 3%) by climate change; GCM modelling uncertainty across scenarios have a higher impact on seasonal VRE variability than climate signals |
| [21] | RCP 4.5 & RCP 8.5 | Y (12 km; hourly but aggregated to daily) | 5 | 1979–2004; 2021–2050; 2061–2090 | Offshore wind | European domain, with a focus on the black sea region | Simplistic: single turbine power curve for the focused area, but a time-varying roughness length is used | Mean wind outputs | Robust signal of decreasing wind over much of the European domain both towards 2050 and 2010, but no discernible negative impact of climate change on wind resources in the Black Sea |
| [60] | RCP 8.5 | Y(12 km; 3 h but aggregated to daily) | 6 | 1971–2000; 2070–2099 | Wind and PV | Europe disaggregated into nine regions | Very simplistic: power law with uniform exponents for wind; three-step power density method for wind; PV conversion does not consider the inclination | Mean wind and PV outputs; wind and solar coefficient of variation and local wind-solar correlation at a time scale from daily, monthly to yearly | The projected changes in local wind-solar temporal correlation are overall negligible (well below ±5%) |
| [40] | RCP 2.6 & RCP 6.0 | N (55 km; daily) | 4 | 1970–2100; 2031–2071; 2070–2100 | Onshore wind, offshore wind, utility PV, rooftop PV | Globe | Very simplistic: Wind and PV conversion are based on yearly mean, without consideration of temporal profiles | Mean wind and PV outputs | Uncertain impacts on the wind with increase and decrease in different regions, and impacts on PV are small |
| [71] | RCP2.6, RCP 4.5 & RCP 8.5 | Y (12 km; 3 h) | 6 | 1986–2006; 2080–2100 | Wind and PV | 33 European countries | Detailed: The multi-turbine power curve is adopted but not location-specific; air density correction is not performed wake losses as a function of wind speed are not considered | Mean wind and PV outputs; the standard deviation of joint wind and PV output ramps | Both wind and solar outputs slightly decrease and their variability increased with the increased strength of climate change |
| [98] | RCP 4.5 & RCP8.5 | Y (12 km; 3 h) | 4 for RCP 8.5 & 1 for RCP4.5 | 1971–2000; 2004–2043 under 1.5 °C; 2016–2059 under 2 °C; 2037–2084 under 3 °C | Wind and PV | 28 European countries | Very simplistic: power law with uniform exponents for wind; three-step power density method for wind; PV conversion does not consider the inclination | Mean wind and PV outputs | Overall reductions in wind and PV outputs for most countries, with less than 5% changes under 1.5 °C and 2 °C conditions; stronger change magnitude for wind under 3 °C conditions, but less than 5% changes remain for most countries. |

(*continued on next page*)

**Table A1** (*continued*)

| Paper | Climate scenario (in terms of RCP) | Whether regional climate model is used (Y/N) for downscaling and associated resolution | Ensemble size per climate scenario | Long-term period studied | Technology (if the wind is not specified as onshore or offshore, it is denoted as wind)or climate variable | Region | Levels of detail of energy conversion model (N.A./Very Simplistic/ Simplistic/Detailed) | Statistical measures | Main conclusion |
|---|---|---|---|---|---|---|---|---|---|
| [52] | 1.5 °C conditions (comparable to RCP1.9 by the end of the century) | N (55 km; daily) | 40 | 2006–2015; a 10-year future period under 1.5 °C | Wind | European domain, with a focus on the UK | Simplistic: power law with uniform exponents for wind; a single turbine power curve is used for wind conversion, using daily mean wind speed with a Rayleigh distribution to factor into sub-daily variation | Mean wind outputs | Increase in wind outputs over much of Europe, with the largest increase over the UK of ~4 pp., but a negligible decrease in wind outputs for Southern Europe; increased variability over much of central and northern Europe where seasonal change is highest in summer |
| [61] | RCP 4.5 & RCP 8.5 | Y (12 km; 3 h) | 5 | 1970–1999; 2070–2099 | PV | Europe disaggregated into nine regions | Simplistic: PV conversion does not consider the inclination | Mean PV outputs; coefficient of variation for solar at timescales from daily, monthly to yearly | PV outputs decrease pronounced in northern countries (up to 12%); but in southern areas, PV outputs and their daily variability slightly increase |
| [15] | RCP 4.5 & RCP 8.5 | N (277.5 km; monthly) | 21 | 2016–2035; 2046–2065; 2081–2100 | Wind | European domain | Very simplistic: theoretical power density method based on surface wind speed | Mean wind outputs | Wind outputs increase in the Northern-Central Europe region but decrease in the Mediterranean region; intra-annual variability increases in the Baltic Sea areas but decreases in the Mediterranean areas and no significant inter-annual variability over Europe |
| [5] | RCP 4.5 & RCP 8.5 | Y (12 km, 3 h) | 6 | 1980–2000; 2045–2065 | Onshore wind and PV | Aggregated Europe and four representative countries (SE, RO, DE, IT) | Simplistic: Only a single turbine power curve is adopted | Mean wind and PV outputs | The ensemble mean suggests a ~ 1% reduction in both wind and solar outputs at aggregated Europe level, but individual ensemble members show inconsistent signs and magnitude of changes. The cross-model uncertainty is exacerbated by seasonal and geographic differences. |
| [24] | RCP 4.5 | N (139 km – 311 km, 12 h) | 36 | 1979–2005; 2020–2049 | Wind | European domain | Simplistic: Only a single turbine power curve is adopted and it does not consider the temporal profiles of wind outputs even if the empirical probability density distribution of wind speeds is used | Mean wind speed and outputs | Annual mean wind speed increases up to 3.5% in northwest Europe and decreases down to −3.5% in south Europe across ensemble members; Mean output change is in line with wind speed change, but more pronounced. The magnitude of changes varies spatially between 12% and 8%. |
| [39] | RCP 4.5 & RCP 8.5 | Y (50 km, 3 h) | 3 for RCP 4.5 & 4 for RCP 8.5 | 1990–1999; 2040–2049 | Onshore wind | China | Simplistic: Both the power law and the logarithmic law are used for wind conversion, but a uniform shear exponent is used for the power law; only a single turbine power curve is adopted | Mean wind outputs; coefficient of variation of wind outputs | Around a 4% reduction in wind outputs for most areas of China, with a 15% increase in south-west China under RCP4.5; wind outputs change under RCP8.5 is similar to RCP4.5, but its increase in Sichuan Basin further shifted to the southeast. |

(*continued on next page*)

**Table A1** (*continued*)

| Paper | Climate scenario (in terms of RCP) | Whether regional climate model is used (Y/N) for downscaling and associated resolution | Ensemble size per climate scenario | Long-term period studied | Technology (if the wind is not specified as onshore or offshore, it is denoted as wind)or climate variable | Region | Levels of detail of energy conversion model (N.A./Very Simplistic/ Simplistic/Detailed) | Statistical measures | Main conclusion |
|---|---|---|---|---|---|---|---|---|---|
| [53] | SSP1-RCP2.6 & SSP5-RCP 8.5 | N (remapped to 277.5 km, daily) | 28 | 1995–2014; 2081–2100 | PV | European domain disaggregated into 156 grid cells | Detailed: However, wind speed's impact on PV efficiency is not considered | Mean PV outputs; cross-correlation of deseasonalized daily PV outputs (standardized by the interannual mean and standard deviation of the same day) | Overall higher PV outputs under RCP 2.6 independent of season or region, except for Scandinavia, Ireland, central-eastern Europe and the Iberian Peninsula; changed seasonal patterns of PV outputs, as outputs increase strongly in winter than in summer under RCP 2.6 or increase in summer and decrease in winter under RCP 8.5; cross-correlation of daily PV outputs in Europe increases the end of the century. |
| [82] | RCP 2.6, RCP 4.5 & RCP 8.5 | N (100 km but downscaled to 1 km using inverse distance-weighting method, monthly but used as scalar for hourly historic observation) | 7 | 2010; 2021–2040; 2041–2060; 2061–2080 | Rooftop PV | Fukushima, Japan | Detailed: Consideration of inclination and the impact of temperature and wind speed on efficiency | Mean PV outputs | PV outputs increase in most cases, which is 0.3%–3.6%, 0.5%–7.0%, 1.5%–9.6% in 2030, 2050 and 2070 approximately |
| [17] | SRES A1B scenario (comparable between RCP 4.5 and RCP 6.0) | N (200 km but statistically downscaled to 5 km, monthly) | 3 | 1980–2010 (only simulated by a weather Research and Forecasting model); 2011–2040; 2041–2070; 2071–2100 | Offshore wind | Taiwan strait | Simplistic: Theoretical power density method based on surface wind speed; using monthly mean wind speed with a Weibull distribution to factor sub-daily variation based on parameters estimated from a Weather Research and Forecasting model | Mean wind outputs | Wind outputs in eastern Taiwan Strait are higher, but reduce slightly by 3% compared with the historic period |
| [99] | RCP 4.5 & RCP 8.5 | Y (12 km, 3 h) | 9 | 1971–2000; 2071–2100 | Wind | Europe disaggregated into nine regions | Very simplistic: power law with uniform exponents for wind; three-step power density method for wind energy conversion | Mean wind outputs; standard deviation of wind outputs from daily, monthly to yearly | Mean wind outputs at aggregated Europe level slightly change in magnitude (±5%); at the regional level the magnitude of change is up to 15% with the Iberian Peninsula being most affected and changes are overall enhanced under RCP 8.5 compared with under RCP 4.5; the standard deviation of wind outputs are small or statistically insignificant across all time scales. |
| [89] | RCP 4.5 & RCP 8.5 | Y (24.4 km, daily) | 22 | 1961–2000; 2021–2061; 2061–2100 | Wind | European domain | Simplistic: power law with uniform exponents for wind; three-step power density method for wind energy conversion; using a probability density function to factor into sub-daily variation | Mean wind outputs | Mean wind outputs increase more likely than not for Northern and Central Europe and likely reduce likely over Southern Europe; a strong increase in seasonal variability for most of Europe; inter-annual variability changes vary between models |

## References


[1] Balla E, Ergen I, Migueis M. Tail dependence and indicators of systemic risk for large US depositories. J Finan Stabil 2014;15:195–209. doi:10.1016/J.JFS.2014.10.002.

[2] Berg P, Almén F, Bozhinova D. HydroGFD3.0 (Hydrological Global Forcing Data): a 25 km global precipitation and temperature data set updated in near-real time. Earth Syst Sci Data 2021;13(4):1531–45. doi:10.5194/ESSD-13-1531-2021.

[3] Berg P, Bosshard T, Yang W, Zimmermann K. MIdASv0.2.1 - Multi-scale bias AdjuStment. Geoscien Model Develop 2022;15(15):6165–80. doi:10.5194/GMD-15-6165-2022.

[4] Bloomfield HC, Brayshaw DJ, Shaffrey LC, Coker PJ, Thornton HE. The changing sensitivity of power systems to meteorological drivers: a case study of Great Britain. Environ Res Lett 2018;13(5):054028. doi:10.1088/1748-9326/AABFF9.

[5] Bloomfield HC, Brayshaw DJ, Troccoli A, Goodess CM, De Felice M, Dubus L, Saint-Drenan YM. Quantifying the sensitivity of european power systems to energy scenarios and climate change projections. Renew Energy 2021;164:1062–75. doi:10.1016/J.RENENE.2020.09.125.

[6] Bobmann T, Staffell I. The shape of future electricity demand: exploring load curves in 2050s Germany and Britain. Energy 2015;90:1317–33. doi:10.1016/J.ENERGY.2015.06.082.

[7] Bódis K, Kougias I, Jäger-Waldau A, Taylor N, Szabó S. A high-resolution geospatial assessment of the rooftop solar photovoltaic potential in the European Union. Renew Sustain Energy Rev 2019;114:109309. doi:10.1016/J.RSER.2019.109309.

[8] Bontemps S, Defourny P, Bogaert EVan, Kalogirou V, Perez JR. GLOBCOVER 2009 products description and validation report. ESA Bull 2011;136:53.

[9] Bosch J, Staffell I, Hawkes AD. Temporally-explicit and spatially-resolved global onshore wind energy potentials. Energy 2017;131:207–17. doi:10.1016/J.ENERGY.2017.05.052.

[10] Bossmann T, Pfluger B, Wietschel M. The shape matters! How structural changes in the electricity load curve affect optimal investments in generation capacity. International Conference on the European Energy Market, EEM; 2013. doi:101109/EEM20136607361.

[11] British Oceanographic Data Centre. (2020). GEBCO Web Services. Retrieved December 5, 2022, from https://www.gebco.net/data_and_products/gebco_web_services/.

[12] Brouwer AS, van den Broek M, Zappa W, Turkenburg WC, Faaij A. Least-cost options for integrating intermittent renewables in low-carbon power systems. Appl Energy 2016;161:48–74. doi:10.1016/J.APENERGY.2015.09.090.

[13] Bruninx, K., Orlic, D., Couckuyt, N., Grisey, N., Betraoui, B., Anderski, T., … Jankowski, R. (2014). E-Highway 2050 Project: D2_1: Data sets of scenarios for 2050. Retrieved July 19, 2022, from http://www.e-highway2050.eu/fileadmin/documents/Results/D2_1_Data_sets_of_scenarios_for_2050_20072015.pdf.

[14] Bussar C, Stöcker P, Cai Z, Moraes L, Magnor D, Wiernes P, Sauer DU. Large-scale integration of renewable energies and impact on storage demand in a European renewable power system of 2050—sensitivity study. J Energy Storage 2016;6:1–10. doi:10.1016/J.EST.2016.02.004.

[15] Carvalho D, Rocha A, Gómez-Gesteira M, Silva Santos C. Potential impacts of climate change on European wind energy resource under the CMIP5 future climate projections. Renew Energy 2017;101:29–40. doi:10.1016/J.RENENE.2016.08.036.

[16] Castillo VZ, Boer HSde, Muñoz RM, Gernaat DEHJ, Benders R, van Vuuren D. Future global electricity demand load curves. Energy 2022;258:124741. doi:10.1016/J.ENERGY.2022.124741.

[17] Chang TJ, Chen CL, Tu YL, Yeh HTe, Wu YT. Evaluation of the climate change impact on wind resources in Taiwan Strait. Energy Convers Manage 2015;95:435–45. doi:10.1016/J.ENCONMAN.2015.02.033.

[18] Chang TP. The Sun's apparent position and the optimal tilt angle of a solar collector in the northern hemisphere. Sol Energy 2009;83(8):1274–84. doi:10.1016/J.SOLENER.2009.02.009.

[19] Copernicus. (2018). CORINE land cover — copernicus land monitoring service. Retrieved July 19, 2022, from https://land.copernicus.eu/pan-european/corine-land-cover.

[20] Copper JK, Sproul AB, Bruce AG. A method to calculate array spacing and potential system size of photovoltaic arrays in the urban environment using vector analysis. Appl Energy 2016;161:11–23. doi:10.1016/J.APENERGY.2015.09.074.

[21] Davy R, Gnatiuk N, Pettersson L, Bobylev L. Climate change impacts on wind energy potential in the European domain with a focus on the Black Sea. Renew Sustain Energy Rev 2018;81:1652–9. doi:10.1016/J.RSER.2017.05.253.

[22] Deng YY, Haigh M, Pouwels W, Ramaekers L, Brandsma R, Schimschar S, de Jager D. Quantifying a realistic, worldwide wind and solar electricity supply. Glob Environ Chang 2015;31:239–52. doi:10.1016/J.GLOENVCHA.2015.01.005.

[23] Densing M, Wan Y. Low-dimensional scenario generation method of solar and wind availability for representative days in energy modeling. Appl Energy 2022;306:118075 October 2021. doi:10.1016/j.apenergy.2021.118075.

[24] Devis A, Van Lipzig NPM, Demuzere M. Should future wind speed changes be taken into account in wind farm development? Environ Res Lett 2018;13(6):064012. doi:10.1088/1748-9326/AABFF7.

[25] Dierauf, T., Growitz, A., Kurtz, S., & Hansen, C. (2013). Weather-corrected performance ratio jose luis becerra cruz weather-corrected performance ratio, (April).

[26] Doelman JC, Stehfest E, Tabeau A, Meijl HVan, Lassaletta L, Gernaat DEHJ, Van Vuuren DP. Exploring SSP land-use dynamics using the IMAGE model : regional and gridded scenarios of land-use change and land-based climate change mitigation. Glob Environ Chang 2018;48:119–35 November 2017. doi:10.1016/j.gloenvcha.2017.11.014.

[27] Dominguez R, Carrion M. Impact of the demand side management in the planning and operations towards 2050. *International Conference on the European Energy Market, EEM, 2019-September*; 2019. doi:101109/EEM20198916414.

[28] Duffie JA, Beckman WA. Solar Engineering of Thermal Processes. Am J Phys 2013;53 John Wiley & Sons, Inc. doi:10.1119/1.14178.

[29] ECMWF. (2022). ERA5 | ECMWF. Retrieved July 13, 2022, from https://www.ecmwf.int/en/forecasts/datasets/reanalysis-datasets/era5.

[30] Erbs DG, Klein SA, Duffie JA. Estimation of the diffuse radiation fraction for hourly, daily and monthly-average global radiation. Sol Energy 1982;28(4):293–302. doi:10.1016/0038-092X(82)90302-4.

[31] EURegulation (EU) 2019/943 of the European Parliament and of the Council of 5 June 2019 on the internal market for electricity. Offic J European Union 2019;62(L158):54–191.

[32] Eurek K, Sullivan P, Gleason M, Hettinger D, Heimiller D, Lopez A. An improved global wind resource estimate for integrated assessment models. Energy Econ 2017;64:552–67. doi:10.1016/J.ENECO.2016.11.015.

[33] European Commission. (2020). *Commission staff working document impact assessment stepping up Europe's 2030 climate ambition*.

[34] European Commission. (2022a). Energy and the green deal. Retrieved January 11, 2023, from https://commission.europa.eu/strategy-and-policy/priorities-2019-2024/european-green-deal/energy-and-green-deal_en.

[35] European Commission. (2022b). Paris agreement. Retrieved January 11, 2023, from https://climate.ec.europa.eu/eu-action/international-action-climate-change/climate-negotiations/paris-agreement_en.

[36] Eurostat. (2022). NUTS Maps - NUTS - nomenclature of territorial units for statistics - Eurostat. Retrieved December 5, 2022, from https://ec.europa.eu/eurostat/web/nuts/nuts-maps.

[37] Fan JL, Hu JW, Zhang X. Impacts of climate change on electricity demand in China: an empirical estimation based on panel data. Energy 2019;170:880–8. doi:10.1016/J.ENERGY.2018.12.044.

[38] Flanders Marine Institute. (2020). Marine Regions. Retrieved December 5, 2022, from https://www.marineregions.org/downloads.php.

[39] Gao, Y., Ma, S., & Wang, T. (2019). The impact of climate change on wind power abundance and variability in China. Energy, 189, 116215. https://doi.org/10.1016/J.ENERGY.2019.116215

[40] Gernaat DEHJ, de Boer HS, Daioglou V, Yalew SG, Müller C, van Vuuren DP. Climate change impacts on renewable energy supply. Nat Clim Chang 2021;11(2):119–25. doi:10.1038/s41558-020-00949-9.

[41] Giarola S, Molar-Cruz A, Vaillancourt K, Bahn O, Sarmiento L, Hawkes A, Brown M. The role of energy storage in the uptake of renewable energy: a model comparison approach. Energy Policy 2021;151:112159. doi:10.1016/J.ENPOL.2021.112159.

[42] Gibescu M, Brand AJ, Kling WL. Estimation of variability and predictability of large-scale wind energy in The Netherlands. Wind Energy 2009;12(3):241–60. doi:10.1002/WE.291.

[43] Giebel, G. (2000). On the benefits of distributed generation of wind energy in Europe.

[44] Gruber S. Derivation and analysis of a high-resolution estimate of global permafrost zonation. Cryosphere 2012;6(1):221–33. doi:10.5194/TC-6-221-2012.

[45] Halpern BS, Frazier M, Afflerbach J, Lowndes JS, Micheli F, O'Hara C, Selkoe KA. Recent pace of change in human impact on the world's ocean. Sci Rep 2019;9(1):1–8 *2019 9:1*. doi:10.1038/s41598-019-47201-9.

[46] Hausfather Z, Peters GP. Emissions – the 'business as usual' story is misleading. Nature 2020;577(7792):618–20. doi:10.1038/d41586-020-00177-3.

[47] Hawkins E, Sutton R. The potential to narrow uncertainty in regional climate predictions. Bull Am Meteorol Soc 2009;90(8):1095–107. doi:10.1175/2009BAMS2607.1.

[48] Held AM. Modelling the future development of renewable energy technologies in the European electricity sector using agent-based simulation. Simulation 2010:196.

[49] Heuberger CF, Staffell I, Shah N, Dowell NMac. A systems approach to quantifying the value of power generation and energy storage technologies in future electricity networks. Comput Chem Eng 2017;107:247–56. doi:10.1016/J.COMPCHEMENG.2017.05.012.

[50] Hoogwijk M. On the global and regional potential of renewable energy sources. Assembly 2004. Retrieved from http://np-net.pbworks.com/f/Hoogwijk+(2004)+Global+and+regional+potential+of+renewable+energy+sources+(Thesis+Utrecht).pdf.

[51] Hoogwijk M, de Vries B, Turkenburg W. Assessment of the global and regional geographical, technical and economic potential of onshore wind energy. Energy Economics 2004;26(5):889–919. doi:10.1016/j.eneco.2004.04.016.

[52] Hosking JS, Macleod D, Phillips T, Holmes CR, Watson P, Shuckburgh EF, Mitchell D. Changes in European wind energy generation potential within a 1.5 °C warmer world. Environ Res Lett 2018;13(5):054032. doi:10.1088/1748-9326/AABF78.

[53] Hou X, Wild M, Folini D, Kazadzis S, Wohland J. Climate change impacts on solar power generation and its spatial variability in Europe based on CMIP6. Earth Syst Dynam 2021;12(4):1099–113. doi:10.5194/ESD-12-1099-2021.

[54] Hu J, Harmsen R, Crijns-Graus W, Worrell E. Geographical optimization of variable renewable energy capacity in China using modern portfolio theory. Appl Energy 2019;253:113614. doi:10.1016/J.APENERGY.2019.113614.

[55] IEA Net zero by 2050: a roadmap for the global energy sector. International Energy Agency; 2021. 224. Retrieved from https://www.iea.org/reports/net-zero-by-2050.

[56] IEC. (2005). IEC 61400-1: wind turbine generator (WTG) Classes.

[57] IPCC Technical summary. in: CLIMATE CHANGE 2013: THE PHYSICAL SCIENCE BASIS.CONTRIBUTION OF WORKING GROUP I TO THE FIFTH ASSESSMENT REPORT OF

THE INTERGOVERNMENTAL PANEL ON CLIMATE CHANGE. Cambridge, United Kingdom and New York, NY, USA: Cambridge University Press; 2013.
[58] IRENA. (2022). *Renewable capacity statistics 2020 Statistiques De Capacité Renouvelable 2020 Estadísticas De Capacidad*.
[59] Isaac M, van Vuuren DP. Modeling global residential sector energy demand for heating and air conditioning in the context of climate change. Energy Policy 2009;37(2):507–21. doi:10.1016/J.ENPOL.2008.09.051.
[60] Jerez S, Tobin I, Turco M, Jiménez-Guerrero P, Vautard R, Montávez JP. Future changes, or lack thereof, in the temporal variability of the combined wind-plus-solar power production in Europe. Renew Energy 2019;139:251–60. doi:10.1016/j.renene.2019.02.060.
[61] Jerez Sonia, Tobin I, Vautard R, Montávez JP, López-Romero JM, Thais F, Wild M. The impact of climate change on photovoltaic power generation in Europe. Nat Commun 2015;6(1):1–8 *2015 6:1*. doi:10.1038/ncomms10014.
[62] Jordan DC, Sekulic B, Marion B, Kurtz SR. Performance and Aging of a 20-Year-Old Silicon PV System. IEEE J Photovol 2015;5(3):744–51. doi:10.1109/JPHOTOV.2015.2396360.
[63] Jurasz J, Canales FA, Kies A, Guezgouz M, Beluco A. A review on the complementarity of renewable energy sources: concept, metrics, application and future research directions. SOL ENERGY 2020;195(November 2019):703–24. doi:10.1016/j.solener.2019.11.087.
[64] Kalogirou SA. *SOLAR ENERGY ENGINEERING: PROCESSES AND SYSTEMS: SECOND EDITION. solar energy engineering: processes and systems: second edition*. Elsevier Inc; 2014. doi:101016/C2011-0-07038-2.
[65] Kan X, Reichenberg L, Hedenus F. The impacts of the electricity demand pattern on electricity system cost and the electricity supply mix: a comprehensive modeling analysis for Europe. Energy 2021;235:121329. doi:10.1016/j.energy.2021.121329.
[66] Kannan R. Dynamics of long-term electricity demand profile: insights from the analysis of Swiss energy systems. Energy Strat Rev 2018;22:410–25. doi:10.1016/J.ESR.2018.10.010.
[67] Katopodis T, Markantonis I, Vlachogiannis D, Politi N, Sfetsos A. Assessing climate change impacts on wind characteristics in Greece through high resolution regional climate modelling. Renew Energy 2021;179:427–44. doi:10.1016/J.RENENE.2021.07.061.
[68] Kjellström E, Nikulin G, Strandberg G, Bøssing Christensen O, Jacob D, Keuler K, Vautard R. European climate change at global mean temperature increases of 1.5 and 2 °C above pre-industrial conditions as simulated by the EURO-CORDEX regional climate models. Earth System Dynam 2018;9(2):459–78. doi:10.5194/ESD-9-459-2018.
[69] Knorr, K. (2016). Modellierung von raum-zeitlichen Eigenschaften der Windenergieeinspeisung für wetterdatenbasierte Windleistungssimulationen, (September). Retrieved from https://kobra.uni-kassel.de/bitstream/handle/123456789/2017020852024/DissertationKasparKnorr.pdf;jsessionid=4F2F5538046EBE15ED39405D4C017443?sequence=7.
[70] Kotlarski, S., Keuler, K., Christensen, O.B., Colette, A., Déqué, M., Gobiet, A., … Wulfmeyer, V. (2014). Regional climate modeling on European scales: a joint standard evaluation of the EURO-CORDEX RCM ensemble. *Geoscien Model Develop*, 7(4), 1297–333. https://doi.org/10.5194/GMD-7-1297-2014
[71] Kozarcanin S, Liu H, Andresen GB. 21st Century climate change impacts on key properties of a large-scale renewable-based electricity system. Joule 2019;3(4):992–1005. doi:10.1016/j.joule.2019.02.001.
[72] Mahlknecht, G. (2013). Greg's cable map. Retrieved December 5, 2022, from https://cablemap.info/_default.aspx.
[73] McKenna R, Hollnaicher S, Ostman P, Fichtner W. Cost-potentials for large onshore wind turbines in Europe. Energy 2015;83:217–29. doi:10.1016/J.ENERGY.2015.02.016.
[74] Meteorological Office UK. (2018). *UKCP18 guidance : representative concentration pathways*.
[75] Miglietta MM, Huld T, Monforti-Ferrario F. Local complementarity of wind and solar energy resources over Europe: an assessment study from a meteorological perspective. J Appl Meteorol Climatol 2017;56(1):217–34. doi:10.1175/JAMC-d-16-0031.1.
[76] Miller L, Carriveau R. Energy demand curve variables – an overview of individual and systemic effects. Sustain Energy Technol Assessments 2019;35:172–9. doi:10.1016/J.SETA.2019.07.006.
[77] Miller LM, Keith DW. Climatic impacts of wind power. Joule 2018;2(12):2618–32. doi:10.1016/J.JOULE.2018.09.009.
[78] NOAA. (2011). Global Gas Flaring Estimates 2006. Retrieved December 5, 2022, from https://www.ncei.noaa.gov/node/2491.
[79] NOAA. (2013). Global DMSP-OLS nighttime lights time series 1992 - 2013 (Version 4). Retrieved December 5, 2022, from https://www.ncei.noaa.gov/node/2321.
[80] Norgaard P, Holttinen H. A multi-turbine power curve approach. In: Nordic Wind Power Conference; 2004. p. 1–2. (March)Retrieved from.
[81] Ohlendorf N, Schill WP. Frequency and duration of low-wind-power events in Germany. Environ Res Lett 2020;15(8). doi:10.1088/1748-9326/ab91e9.
[82] Oka K, Mizutani W, Ashina S. Climate change impacts on potential solar energy production: a study case in Fukushima, Japan. Renew Energy 2020;153:249–60. doi:10.1016/J.RENENE.2020.01.126.
[83] Otero Felipe N, Martius O, Allen S, Bloomfield H, Schaefli B. A copula-based assessment of renewable energy droughts across Europe. SSRN Electronic J 2022. doi:10.2139/ssrn.3980444.
[84] Peyrard, C. (2015). Offshore wind turbine foundations EDF R&D-LNHE Laboratoire d'Hydraulique St Venant.
[85] pvxchange.com. (2022). Sanyo HIP-225HDE1. Retrieved July 20, 2022, from https://www.pvxchange.com/Solar-Modules/Sanyo/HIP-225HDE1_1-2100492.
[86] Raynaud, D., Hingray, B., François, B., & Creutin, J.D. (2018). Energy droughts from variable renewable energy sources in European climates. *Renew Energy*, 125, 578–89. https://doi.org/10.1016/J.RENENE.2018.02.130
[87] Reich NH, Mueller B, Armbruster A, van Sark WGJHM, Kiefer K, C R. Performance ratio revisited: is PR > 90% realistic? PROG PHOTOVOLTAICS RES APPL 2012;20:717–26. doi:10.1002/pip.1219.
[88] Remke T. ASSESSING CLIMATE CHANGE IMPACTS ON WIND ENERGY FINANCING. Universitätsbibliothek der Leuphana Universität Lüneburg; 2020.
[89] Reyers M, Moemken J, Pinto JG. Future changes of wind energy potentials over Europe in a large CMIP5 multi-model ensemble. Int J Climatol 2016;36(2):783–96. doi:10.1002/JOC.4382.
[90] Riahi K, Rao S, Krey V, Cho C, Chirkov V, Fischer G, Rafaj P. RCP 8.5-a scenario of comparatively high greenhouse gas emissions. Clim Change 2011;109(1):33–57. doi:10.1007/S10584-011-0149-Y/FIGURES/12.
[91] Schindler D, Behr HD, Jung C. On the spatiotemporal variability and potential of complementarity of wind and solar resources. Energy Convers Manage 2020;218(May):113016. doi:10.1016/j.enconman.2020.113016.
[92] Sliz-Szkliniarz, B. (2013). *Energy planning in selected European regions: methods for evaluating the potential of renewable energy sources*.
[93] Soares PMM, Lima DCA, Cardoso RM, Nascimento ML, Semedo A. Western Iberian offshore wind resources: more or less in a global warming climate? Appl Energy 2017;203:72–90. doi:10.1016/J.APENERGY.2017.06.004.
[94] Staffell I, Green R. How does wind farm performance decline with age? Renew Energy 2014;66:775–86. doi:10.1016/j.renene.2013.10.041.
[95] Staffell I, Pfenninger S. Using bias-corrected reanalysis to simulate current and future wind power output. Energy 2016;114:1224–39. doi:10.1016/J.ENERGY.2016.08.068.
[96] Staffell I, Pfenninger S. The increasing impact of weather on electricity supply and demand. Energy 2018;145:65–78. doi:10.1016/J.ENERGY.2017.12.051.
[97] Svenningsen, L. (2010). Power curve air density correction and other power curve options in windPRO.
[98] Tobin I, Greuell W, Jerez S, Ludwig F, Vautard R, Van Vliet MTH, Breón FM. Vulnerabilities and resilience of European power generation to 1.5 °C, 2 °C and 3 °C warming. Environ Res Lett 2018;13(4):044024. doi:10.1088/1748-9326/AAB211.
[99] Tobin Isabelle, Jerez S, Vautard R, Thais F, Van Meijgaard E, Prein A, Teichmann C. Climate change impacts on the power generation potential of a European mid-century wind farms scenario. Environ Res Lett 2016;11(3). doi:10.1088/1748-9326/11/3/034013.
[100] Tobin Isabelle, Vautard R, Balog I, Bréon FM, Jerez S, Ruti PM, Yiou P. Assessing climate change impacts on European wind energy from ENSEMBLES high-resolution climate projections. Clim Change 2015;128(1–2):99–112. doi:10.1007/S10584-014-1291-0/FIGURES/3.
[101] UNEP-WCMC and IUCN. (2020). Protected planet: the world database on protected areas (WDPA). Retrieved December 5, 2022, from https://www.protectedplanet.net/en/thematic-areas/wdpa?tab=WDPA.
[102] United Nations. (2022). All about the NDCs. Retrieved July 7, 2022, from https://www.un.org/en/climatechange/all-about-ndcs.
[103] United States Geological Survey. (2018). Digital elevation - global 30 arc-second elevation (GTOPO30). Retrieved May 3, 2022, from https://rda.ucar.edu/datasets/ds758.0/.
[104] van Zuijlen B, Zappa W, Turkenburg W, van der Schrier G, van den Broek M. Cost-optimal reliable power generation in a deep decarbonisation future. Appl Energy 2019;253:113587. doi:10.1016/J.APENERGY.2019.113587.
[105] Vuuren, D.P.Van, Kriegler, E., & Neill, B.C.O. (2014). A new scenario framework for climate change research : scenario matrix architecture, 373–86. doi:10.1007/s10584-013-0906-1.
[106] Wind turbine models.com. (2014). Vestas V105-3.3 - 3,30 MW - wind turbine. Retrieved December 5, 2022, from https://en.wind-turbine-models.com/turbines/891-vestas-v105-3.3
[107] Wind turbine models.com. (2015a). Vestas V117-3.3 - 3,30 MW - wind turbine. Retrieved December 5, 2022, from https://en.wind-turbine-models.com/turbines/694-vestas-v117-3.3
[108] Wind turbine models.com. (2015b). Vestas V126-3.3 - 3,30 MW - wind turbine. Retrieved December 5, 2022, from https://en.wind-turbine-models.com/turbines/695-vestas-v126-3.3.
[109] Wind turbine models.com. (2015c). Vestas V164-8.0 - 8,00 MW - wind turbine. Retrieved December 5, 2022, from https://en.wind-turbine-models.com/turbines/318-vestas-v164-8.0.
[110] Yang, Y., Javanroodi, K., & Nik, V.M. (2022). Climate change and renewable energy generation in Europe—long-term impact assessment on solar and wind energy using high-resolution future climate data and considering climate uncertainties. *Energies 2022, Vol. 15, Page 302*, 15(1), 302. doi:10.3390/EN15010302.
[111] Zappa W, van den Broek M. Analysing the potential of integrating wind and solar power in Europe using spatial optimisation under various scenarios. Renew Sustain Energy Rev 2018;94(August):1192–216. doi:10.1016/j.rser.2018.05.071.
[112] Zhang H, Chen B, Li Y, Geng J, Li C, Zhao W, Yan H. Research on medium- and long-term electricity demand forecasting under climate change. Energy Rep 2022;8:1585–600. doi:10.1016/J.EGYR.2022.02.210.
[113] Hausfather Z, Ritchie J. (2019). A 3C World Is Now "Business as Usual", https://thebreakthrough.org/issues/energy/3c-world.